Centrifuge Modeling of the Installation Advancement Ratio Effect on the Cyclic Response of a Single-Helix Screw Pile for Floating Offshore Wind

Wang, Wei; Brown, Michael; Sharif, Yaseen Umar; Davidson, Craig; Ciantia, Matteo Oryem

Published in:
Journal of Geotechnical and Geoenvironmental Engineering

DOI:
10.1061/JGGEFK.GTENG-12331

Publication date:
2025

Document Version
Peer reviewed version

Centrifuge modelling of the installation advancement ratio effect on the cyclic response of a single-helix screw pile for floating offshore wind

Wei Wang[1]; Michael John Brown, Ph.D.[2]; Yaseen Umar Sharif[3]; Craig Davidson[4]; Matteo Oryem Ciantia, Ph.D.[5]

*Corresponding author
*Wei Wang, BSc, MSc
PhD student, School of Science and Engineering, University of Dundee, Fulton Building, Dundee, DD1 4HN, UK
ORCID: 0000-0002-3838-2142
Email: 2422030@dundee.ac.uk

Prof Michael John Brown, BEng (Hons), PhD, GMICE
Professor of Geotechnical Engineering, School of Science and Engineering, University of Dundee, Fulton Building, Dundee, DD1 4HN, UK
ORCID: 0000-0001-6770-4836
Email: m.j.z.brown@dundee.ac.uk

Mr Yaseen Umar Sharif, MEng (Hons), GMICE
Research Associate, School of Science and Engineering, University of Dundee, Fulton Building, Dundee, DD1 4HN, UK
ORCID: 0000-0002-3620-7500
Email: y.sharif@dundee.ac.uk

Mr Craig Davidson, BSc (Hons), MSc, GMICE
Geotechnical Engineering Facility Manager, School of Science and Engineering, University of Dundee, Fulton Building, Dundee, DD1 4HN, UK
ORCID: 0000-0002-4843-5498
Email: c.s.davidson@dundee.ac.uk

Dr Matteo Oryem Ciantia, PhD, GMICE
Senior Lecturer, School of Science and Engineering, University of Dundee, Fulton Building, Dundee, DD1 4HN, UK
ORCID: 0000-0003-1897-4471
Email: m.o.ciantia@dundee.ac.uk

Abstract

Upscaled screw piles have been proposed as anchors for offshore floating wind applications, but this upscaling can result in a significant increase in vertical installation forces. Previous studies have shown that the use of over-flighting techniques during installation (installation advancement ratio, AR < 1.0) can reduce or eliminate these forces and improve the capacity and stiffness of screw piles under monotonic tensile loading conditions. However, the impact of over-flighting installation on the cyclic response of screw piles has not received adequate attention. To address this, a series of drained cyclic uplift tests in a geotechnical centrifuge were conducted. The tests involved different AR values during installation and varying one-way cyclic tensile loading amplitudes. The results revealed that reducing the installation AR can significantly decrease displacement accumulation and improve cyclic loading stiffness, resulting in a more stable cyclic response. The cyclic axial loading stiffness tends to stabilize or slightly decrease with cycling for stable cases, whilst unstable and meta-stable

cases exhibit an initial reduction of loading stiffness followed by a stabilization or slow recovery. The post-cyclic monotonic uplift tests also show that capacity degradation was predominately due to the displacement accumulation itself rather than any additional cyclic effects. The cyclic stability of the screw pile investigated was found to be comparable with straight-shafted and screw piles from previous studies and beneficial installation effects were maintained under cyclic loading. A predictive framework for displacement accumulation and capacity degradation is also presented and developed within this paper.

Author keywords: screw pile; helical anchor; cyclic loading; installation effect

Introduction

Screw piles (also referred as to helical piles) consist of one or several helices connected to a central straight shaft or core (Perko 2009) and are typically installed by applying torque and vertical (crowd) force simultaneously at the pile head. Screw piles have been widely used onshore (Cerato and Victor 2014; Lutenegger 2011; Schiavon et al. 2019b) and have been suggested as an innovative solution for foundations/anchors for offshore wind turbines (Cerfontaine et al. 2023b; Davidson et al. 2022; Spagnoli and Tsuha 2020). Compared to driven straight shafted piles, screw piles have three main advantages. Firstly, the bearing mechanism formed due to the helix potentially leads to improved tensile/compressive capacity compared to straight shaft piles with the same shaft diameters (Cerfontaine et al. 2021b). Secondly, the rotational installation is more environmentally friendly as it can reduce noise and vibration which is considered potentially detrimental to marine animals (Herbert-Read et al. 2017). Finally, screw piles have the potential to be decommissioned by reverse rotation (Ding et al. 2019).

Based on rotation speed and vertical penetration rates, the installation of screw piles can be described using the term advancement ratio (AR) (Sharif et al. 2021a), which is defined as the ratio of the vertical penetration per rotation to the helix pitch:

$$AR = \frac{\Delta_z}{p_h} \qquad 1$$

where Δ_z is the vertical displacement per rotation and p_h is the pitch of the helical plate i.e. the vertical distance between the top and the bottom of a single helix (see Figure 1). Current standards e.g. BS8004 (British Standards Institution 2015) recommend that, for optimized in-service performance, a pitch-matched installation (AR=1) should be employed with a

tolerance of ± 0.15 to minimize the 'disturbance' of the in-situ soil as 'disturbance' is typically considered to be detrimental to pile performance.

To enable offshore application for wind energy, screw piles need to be upscaled over and above the sizes typically used onshore. Davidson et al. (2022) suggested that the typical helix diameter ranging from 150 to 600 mm onshore (Perko 2009) may need to increase to over 3 m for offshore use to replace single driven piles in fixed wind turbine jacket structures. This upscaling, however, may lead to prohibitively high vertical installation force of up to tens of MN, if pitch-matched installation is used. Fortunately, recent studies in sand have shown that over-flighting (AR < 1.0) during installation has the potential to reduce the required vertical installation force and, contrary to the published guidance, may improve the in-service tensile response, although probably at the expense of compressive performance (Cerfontaine et al. 2022; Cerfontaine et al. 2021a; Sharif et al. 2021a). This phenomenon makes over-flighted screw piles attractive for use as anchors in sand for floating wind where tensile loads predominate. However, the improved tensile capacity due to over-flighted installation has only been observed in sand to date and further verification for other soil conditions e.g. clay is required (Ullah et al. 2023).

Figure 1 illustrates how the state of the soil around the screw pile changes during pitch-matched and over-flighted installation in sand. The pitch-match installation (Figure 1a) theoretically causes least displacements of soil particles around the pile, but previous studies using DEM (Cerfontaine et al. 2021a; Sharif et al. 2021a) and experiments with image-based technologies (such as Schiavon (2016) who 3D scanned the soil bed after the installation of a screw pile) have shown that soil within a radial distance of two helix diameters (D_h) from the pile is significantly loosened when the helix penetrates through it. This loosening results in a reduction of relative density (D_r) and average effective stress (σ_p') of the soil above the helix. In addition, Figure 1(a) shows that, similar to pushing in a straight-shafted pile, a zone with increased D_r and σ_p' is generated below the helix and pile tip (Zhang and Wang 2015). In contrast, as shown in Figure 1(b), by over-flighting (same pile head penetration rate but greater rotation rate), similar to a screw conveyor or Archimedes screw, the helix picks up particles and displaces them upward. This installation approach does 'disturb' or displace the surrounding soil more but leads to densification and stress increase of the soil above the helix (Cerfontaine et al. 2023a; Sharif et al. 2021a). This process can partially recover the degradation of soil due to the helix penetration and may even improve the soil above the helix compared to the virgin conditions before pile installation. However, upward soil movement through the helix due to over-flighting installation can reduce D_r and σ_p' of the zone below the helix. From a mechanical point of view, it is the increase of stress in the soil above the helix combined with the decrease of the stress in the soil below the helix that results in a reduction of compressive resistance during installation. Therefore, less installation vertical force is required for over-

flighting installation than pitch-matched installation. In terms of in-service tensile performance, both the shaft and helix component can be improved by over-flighting. For the helix response, the greater tendency of dilation associated with increased relative density, D_r leads to a wider failure mechanism at the soil surface (Sharif et al. 2021a) and the increased normal stress on the failure surface enhances the unit friction resistance (Cerfontaine et al. 2019). Furthermore, the increased D_r along with the enhanced radial stress around pile shaft can improve the shaft response. However, the effects of installation AR have not been considered in any design methods to date.

Offshore foundations/anchors also need to be able to perform under cyclic loading from wind, waves and loads induced by the operation of the specific structural application. Therefore, any cyclic loading induced displacement accumulation and capacity evolution is a concern for design and application in offshore renewable energy anchoring applications. Cyclic tensile response of (straight shafted) driven piles for offshore wind has been widely reported and it has been suggested that the pile response to cyclic loading depends on multiple factors e.g. loading scenarios (cycle number *N*, loading amplitude Q_{cyc} and mean loading Q_{mean}) (Puech and Garnier 2017). For straight-shafted piles, there are many studies that have revealed that high amplitude axial force cycles can cause considerable reduction of capacity and loading stiffness at the pile shaft-soil interface, as well as permanent pile displacement, due to the pile shaft-soil interface contraction with increasing cycle numbers. As well as the magnitude of cyclic loading, the cyclic behavior has also been shown to be affected by pile geometry and ground conditions (Mortara et al. 2007; Rimoy et al. 2022). For example, pile shaft - sand interface element tests undertaken by Mortara et al. (2004) showed that higher initial normal stress led to lower shaft capacity degradation rates. Poulos (1989) and Puech and Garnier (2017) suggested that displacement piles, where enhanced stresses is created as a result of the mode of installation, are more stable than non-displacement piles in sand. These observations on straight-shafted piles imply that the enhanced radial stress around the shaft of a screw pile due to over-flighting (Sharif et al. 2021a) may also improve the cyclic stability. The cyclic end bearing performance of a solid pile in compression could be assumed as an analogue to some elements of the helix behavior. For example, for closed ended straight shafted piles the end resistance tends to reduce with fixed-amplitude displacement cycles due to a gap created between the pile end and soil below (Galvis-Castro et al. 2023; Le Kouby et al. 2004). Whilst in force-controlled regimes it has been found that the end bearing resistance component tends to increase due to a reduction in the shaft resistance as mentioned above to achieve a constant target total force (Le Kouby et al. 2004), although cyclic performance is likely to be dominated by the pile shaft as would be expected based upon the differences in stiffness and mobilization behavior between shaft and end bearing (or helix in this case) (Fleming et al. 2009). In terms of a screw pile this may suggest that under cyclic force loading regimes there will be load transition from the shaft to the helix.

In contrast to straight-shafted piles, only a limited number of studies have evaluated cyclic performance of screw piles. For example, Newgard et al. (2015) performed 1g experiments on model single-helix screw piles (helix diameter D_h > 152 mm) at shallow installation depths (H/D_h = 3.0 to 5.5, where H is helix embedment depth ranging from 460 mm to 840 mm) in saturated medium dense sand. Schiavon et al. (2019a) undertook centrifuge tests on single helix screw piles installed in very dense sand ($D_r \approx 99\%$) at a greater depth (H/D_h = 7.4, D_h =330 mm and H = 2440 mm at prototype scale). Both studies concluded that higher cyclic amplitudes Q_{cyc} lead to greater displacement accumulation rates. Hao et al. (2022) undertook 1g experiments on small model single-helix screw piles (D_h = 50 mm) deeply embedded (H/D_h = 12). They suggested significant increase of axial loading stiffness for the first or first tens of cycles if the accumulated pile uplift displacement (d_{za}) did not exceed $0.1D_h$ within 100 cycles. In addition, they showed that the post-cyclic tensile capacity $Q_{t\_postcyc}$ fluctuated between 85% and 110% of pre-cyclic tensile capacity Q_t as long as d_{za} remained lower than approximately 0.12 D_h. However, with further displacement accumulation, $Q_{t\_postcyc}$ tended to decrease. Similar observations regarding loading stiffness and post-cyclic capacity were also made by Schiavon et al. (2019a). These studies focused on smaller onshore piles and only pitch matched installation (or did not address the control of installation) was investigated.

The effects of advancement ratio on cyclic performance have also received some limited attention. Wang et al. (2021) numerically investigated cyclic performance of a screw pile installed in sand (D_r = 52%) at varying AR using discrete element modelling (DEM). The results suggested that installing screw piles at lower AR values (0.5 and 0.25) can reduce displacement accumulation caused by one-way cyclic tensile loading compared to pitch-matched installation (AR = 1.0). Wang et al. (2023b) conducted limited centrifuge experiments to validate the reduction in cyclic displacement accumulation due to over-flighting. In these experiments, the piles were subjected to $Q_{cyc} = Q_{mean}$ = 28.6% of tensile capacity Q_t at AR = 1.0. The pile installed at AR = 1.0 only required 8 cycles to reach an accumulated displacement of $d_{za} = 0.1D_h$, while the pile installed at AR = 0.25 required 900 cycles to reach the same displacement.

As Wang et al. (2023b) only investigated a certain absolute magnitude of cyclic loading when varying AR it remains unclear if the observed improvement in cyclic response was only related to the improved tensile capacity or over-flighting affects the resulting mechanisms under cyclic loading. Therefore, additional studies are required to address the dearth of information with respect to screw pile cyclic performance and installation effects and to demonstrate this piling technology and how it can be optimized for field deployment. To give more confidence in the beneficial effects of over-flighting on cyclic and post-cyclic performance, a series of drained centrifuge tests were used to study the cyclic response of a single-helix screw pile, which was installed at AR varying from 0.25 to 1.0 in dry medium-dense sand. The overall cyclic response

was investigated in terms of accumulated uplift displacement, loading stiffness, and post-cyclic capacity. Cyclic stability is also discussed with respect to the performance of straight shafted piles and smaller diameter screw piles typically used in onshore practice. Initial prediction frameworks for accumulated displacement and capacity loss induced by cyclic loading are proposed as part of this study.

Methodology

Centrifuge Setup

Pile testing was conducted in a strong box filled with dry sand on the University of Dundee's 3m radius geotechnical beam centrifuge. The aim of this study was to model drained behavior of piles in high permeability soil (i.e., no excess pore pressure development around the pile during installation or loading). Therefore, these experiments were conducted in dry sand. Effective stress at 80g conditions in saturated sand was simulated by operating the centrifuge at 50g in dry sand, so the dimensional scaling factor in this study was set at 80 (Davidson et al. 2022; Li et al. 2010). This approach is explained in more detail as per Li et al. (2010) where in saturated sand, the effective vertical stress of soil is expressed as:

$$\sigma_v' = \rho' g_{sat} z \qquad 2$$

where g_{sat} is the acceleration in a centrifuge test in saturated sand e.g. g_{sat} = 80g; ρ' is the buoyant density of the saturated sand (1013 kg/m^3) and z is the depth of the soil in an 1/80 scale model. To achieve the equivalent soil conditions, the vertical stress of dry sand expressed in Eq. 2 should be equal to the effective vertical stress of saturated sand in Eq. 3:

$$\sigma_v' = \rho_d g_d z \qquad 3$$

where g_d is the acceleration to be imposed in a centrifuge test on dry sand; ρ_d= the dry density of the sand (1631 kg/m^3), and z = the depth of soil in scale model. Thus, the g_d value is 50g, obtained by equation 3:

$$g_d = \frac{\rho'}{\rho_d} . g_{sat} = 50g \qquad 4$$

This approach was further validated and adopted by Klinkvort and Hededal (2013) who undertook centrifuge testing of monopiles in both dry and saturated soil beds and report virtually no difference between the two approaches to testing.

Since the installation effect is the focus of this study, ensuring the correct post-installation stress field is a major concern for correct modelling. Previous centrifuge studies considered wished-in-place (WIP) piles (Hao et al. 2019) where installation effects were not accounted for. Installation of piles at 1g and then loading the pile in-flight in the centrifuge has also been adopted e.g. Rafsanjani et al. (2021), but this leads to a significantly "softer" in-service loading response and reduced capacity (Al-Baghdadi 2018; Ko et al. 1984) as insertion occurs under very different stress conditions. To create a realistic post-installation stress field and maintain this during load testing, installation and loading were undertaken in one continuous centrifuge operation (inflight) using a purpose built two axis actuator controlled by two servo-motors which precisely control the rotational and vertical displacement of the model piles. During installation and loading events both forces and torques were continuously measured by a combined axial force – torque load cell (F310-Z, Novatech Measurements Ltd.) rigidly connected to the pile head. The load cell was capable of measuring torque to $\pm$30 Nm and axial force to $\pm$20 N. More details of the actuator can be found elsewhere (Davidson et al. 2018; Wang et al. 2023b).

Soil Bed Preparation

Medium-dense soil beds ($D_r \approx$ 50%, 434 mm deep) were created by dry pluviation of HST95 sand (Lauder 2010) in a 500 mm × 800 mm × 550 mm strong box used for the tests. HST95 sand is a fine-grained quartz sand that has been extensively used and characterized at the University of Dundee for laboratory testing. Properties of HST95 sand are given in Table 1.

The soil beds were created by dry pluviation using a slot pluviator (Ueno 1998). The pluviator was automated and designed to move back and forth at a constant speed on rails with the pluviator set 1.5 m above the bottom of the strong box and 1.1 m above the final soil surface. The slot width of 4.5 mm and pluviator sweeping speed of 160 mm/s were adopted to achieve the target D_r = 50% based upon previous calibration studies. The soil density was checked by means of density pots installed during pluviation and recovered after testing for verification. The sand was pluviated to slightly above the target height, and then the sand surface was carefully levelled near surface only.

Pile Model

The steel screw pile used comprised of a solid core with 11 mm diameter (D_s), a 21.25 mm diameter helical plate (D_h) and 7 mm helix pitch (p_h) (model scale) (Figure 2). The solid pile core (shaft) was adopted to avoid structural failure and to simulate an assumed worst-case scenario of the pile plugging during installation. The helix plate thickness was set at 1.4 mm as a compromise between true scaling and structural integrity. This pile geometry has been widely used as a benchmark for AR effects studies at the University of Dundee (Cerfontaine et al. 2023a; Cerfontaine et al. 2021a; Davidson et al. 2022; Sharif et al. 2021a; Sharif et al. 2021b). Using a single helix pile minimizes torque requirements for installation and enables

a preliminary understanding of AR effects on cyclic performance to be obtained without potentially complicated interaction between helices occurring during installation and loading tests (Wang et al. 2023a). The pile installation depth was L = 160 mm, resulting in helix embedment depth of $H = 7.4D_h$ which corresponded a shallow mechanism in uplift but was close to the transition from a shallow to a deep failure mechanism (Cerfontaine et al. 2019).

The ratio of pile shaft diameter to mean sand particle diameter D_s/d_{50} was 57, which is larger than recommendation of 44 for straight-shafted piles (Garnier et al. 2007). The ratio of effective helix width ((D_h - D_s) / 2) to d_{50} was 36, which is also higher than recommendation of 16 for screw piles (Rafsanjani et al. 2021; Schiavon et al. 2016).

Two tests were conducted in each box. After the first test, the centrifuge was spun down followed by the pile removal at a constant velocity of 50 mm/min (at 1g). Then the actuator was repositioned manually, before centrifuge spin up for the second test. The shortest distance from the pile to the box boundary was 250 mm ($11.8D_h$) and the distance between the two installation positions was 300 mm ($14.1D_h$), which were chosen to avoid boundary or pile interaction effects (Bolton et al. 1999).

Pile Installation

After spinning up to 50g, the force and torque values induced by the pile self-weight were set to zero (Figure 3a and b). This was then followed by pile installation at a constant rotation rate (3 revs/min) and a constant vertical velocity was chosen to impose the desired AR. Once the pile helix reached the target depth, the vertical and rotational movements were stopped simultaneously. Then the applied torque was released, which in turn modified the vertical force measured at the end of the installation. Rotation of the pile was then fixed again, and subsequent loading tests were conducted.

The pile was installed at AR=1.0, 0.5 and 0.25 to cover a broad range of AR and cover the critical AR and pitch matched situation. AR = 1.0 corresponded to conventional pitch-matched installation. Assuming the soil is incompressible and based upon the condition where the pile shaft (core) penetration volume is equal to soil volume displaced upwards by the helix (Viggiani 1989), Cerfontaine et al. (2023a) proposed a critical AR value (AR_{cr}, Eq. 5) :

$$AR_{cr} = \left[1 - \left(\frac{D_s}{D_h}\right)^2\right]\left(1 - \frac{t_h}{p_h}\right) \qquad 5$$

The AR_{cr} calculated for the pile in this study is 0.64 which suggests that at an AR = 0.5 the pile would be able to create tensile forces during installation and will be able to effectively pull itself into the ground creating minimal crowd force requirements.

Loading Tests

To determine the original monotonic tensile capacity of the pile before subjecting it to cyclic loading Q_t, monotonic tests were conducted on the pile installed at varying AR values, where the pile was monotonically uplifted to a maximum displacement of 40%D_h (8.5mm) at a constant velocity of 1 mm/s (Figure 3a).

To apply the vertical tensile cyclic loading to the screw pile (Figure 3b), a proportional-integral-derivative (PID) controller was used. More details of the PID system can be found elsewhere (Wang et al. 2023b). For the pile loaded cyclically (Figure 4), the applied cyclic loading in this study was force controlled and followed a sinusoidal wave form with a period of 10s. As the target application is offshore floating wind applications, only tensile one-way loading regimes were investigated. For simplification, the amplitudes Q_{cyc} of all loading regimes studied were equivalent to the mean value of loading Q_{mean}hence minimum loading Q_{min} = 0 (Figure 4). After the cyclic loading phase, a monotonic pullout test, to determine the post-cyclic capacity $Q_{t\_postcyc}$, was performed using the same procedure used to determine Q_t as illustrated in Figure 3b.

Cyclic Stability Criteria and Testing Program

Jardine and Standing (2012) summarized the ICP (Imperial College Pile) field tests on straight shafted piles and characterized the overall cyclic response of piles using cyclic interaction diagrams (also referred to as cyclic stability diagrams). Similar to Jardine and Standing (2012) and Schiavon (2016), the current study defines the three modes of overall cyclic response as:

I) Unstable (US): pile head accumulated displacement d_{za} (see Figure 5) increases rapidly and reaches an ultimate displacement of 10%D_h within 100 cycles.

II) Stable (S): pile sustained at least 1000 cycles, displaced by less than ultimate displacement of 10%D_h at rates no more than Δd_{za} = 0.003%D_h (see Figure 5), without noticeable loss in tensile capacity.

III) Meta-stable (MS): pile head displacement accumulates to 10%D_h in 100 to 1000 cycles at rates no more than Δd_{za} = 0.03%D_h.

Table 2 summarizes loading regimes and main results of all the cases studied. In the pile identification nomenclature, letter 'C' and 'M' indicate monotonic and cyclic loading tests respectively, followed by value of installation AR and where relevant the loading amplitude in MN at prototype scale if it was a cyclic test. Three AR values were investigated, and a single monotonic test was conducted at each AR value to determine the monotonic (M) tensile response (M1.0, M0.5 and M0.25). Cyclic (C) tests C1.0-1.6, C0.5-1.6 and C0.25-1.6 had an equal absolute loading amplitude Q_{cyc} of 1.6 MN (21.2%

to 28.6% normalized by monotonic capacity Q_t), which was adopted based upon previous centrifuge tests and DEM simulations (Wang et al. 2021; Wang et al. 2023b) as it led to unstable behavior of screw piles installed at AR = 1.0 and meta-stable behavior of AR = 0.5 and 0.25, for the specific pile geometry and ground conditions studied. Since the variation of AR creates different monotonic capacity, C0.5-1.92 and C0.25-2.17 had loading amplitudes of 1.92 MN and 2.17 MN, respectively, to match the equal normalized loading amplitude of Q_{cyc} = 28.6%Q_t adopted in the pitch-matched case C1.0-1.6. Tests C1.0-0.77, C0.5-0.88, C025-1.03 and C1.0-0.39 with lower Q_{cyc} = 13.5%Q_t, were designed to observe stable behavior. As C1.0-1.6 exhibited an unstable behavior, a pitch-matched case with even lower Q_{cyc} = 6.7%Q_t (C1.0-0.39) was added. As suggested by Zheng et al. (2019) the larger Q_{cyc} (20% ~ 30%Q_t) tends to represent design storm conditions, whilst the lower Q_{cyc} (6.7%~13.5%Q_t) would correspond to normal wave conditions for a straight shafted pile. Except for test C1.0-0.77, in which the pile was pulled out as the pile capacity dropped to below the applied loading and head accumulated displacement d_{za} reached 0.4D_h at the end of cycling, the remaining cases were stopped once d_{za} reached the ultimate value of 0.1D_h or the cycle number N reached 1000.

Results and Discussion

Installation and Monotonic Uplift Tests

Figure 6(a) shows a noticeable reduction in vertical installation force required as AR decreases. By reducing AR from 1.0 to 0.25, the input vertical force at the end of the installation decreased from 8.3 MN to – 2.9 MN, indicating that the pile was in tension and that the motor did not push the pile down but instead needed to resist the downward pull-in force from the pile to maintain the installation velocity. Whilst for AR = 0. 5 the nearly net zero force throughout installation suggests that the pile was neither in tension nor compression. This is close to a condition where the pile is rotating itself into ground with torque input under its own self-weight where this value is close to the critical value predicted by Eq. 5.

In terms of magnitude, installation torque (Figure 6b) varied less with AR but the over-flighting had an impact on the shape of the of torque-installation depth relationship. For the pitch-matched case (AR = 1.0), torque linearly increased with depth. However, reducing AR resulted in non-linear relationship between torque and depth, leading to lower torque at shallow depth and higher torque at greater depth.

Figure 7(a) shows the monotonic uplift response with varying AR. It indicates that the tensile capacity Q_t, which is defined as the maximum or peak resistance, increased with reducing AR. The tensile capacity Q_t was 5.66 MN, 6.79 MN and 7.58 MN for AR = 1.0, 0.5 and 0.25, respectively. In addition, the initial stiffness increases significantly with reducing AR. For AR = 1.0, the tensile resistance increased gradually and reached the maximum at the displacement of 0.15D_h. Whilst for

AR = 0.5 and 0.25, the tensile resistance reached the maximum almost immediately as the pile was subjected to the monotonic tensile and the resistance was maintained up to a displacement of $0.1D_h$, after which the resistance started to reduce significantly. Similar observations on installation requirements and monotonic tensile response have been made by others (Cerfontaine et al. 2022; Cerfontaine et al. 2023a; Sharif et al. 2021a; Sharif et al. 2021b; Wang et al. 2023a; Wang et al. 2023b).

Cyclic Displacement Accumulation

Figure 8 presents the accumulated displacement response with cycles. Figure 8(a) compares the response of the pile subjected to an equal absolute loading (Q_{cyc} = 1.6 MN, 21.2% to 28.6%Q_T for AR = 0.25 to 1.0, respectively), showing that the pitch-matched pile reached ultimate displacement within 10 cycles exhibiting an unstable behavior (US), whereas the pile installed at AR = 0.5 (lasting 500 cycles) and 0.25 (lasting 900 cycles) exhibited better meta-stable (MS) performances. However, this improvement is at least partially attributed to the enhanced tensile capacity due to over-flighting because the applied cyclic normalized loading amplitude reduces with over-flighting (reducing AR). By comparing the displacement response of the pile subject to the same normalized loading (Q_{cyc} = 28.6%Q_T, 1.6 MN to 2.17 MN for AR = 1.0 to 0.25, see Figure 8b), it is suggested that the displacement accumulation of AR = 0.5 and 0.25 was still significantly smaller than that of AR = 1.0, reaching the ultimate displacement after 88 cycles (US) and 400 cycles (MS), respectively. Thus, some caution is required with screw piles when normalizing cyclic behavior as the ultimate resistance changes depending on the installation approach used.

Figure 8(c) indicates that, when the applied loading amplitude was reduced to Q_{cyc} = 13.5%Q_T, the pitch-matched pile still accumulated displacement quickly and could not last for more than 60 cycles. However, in contrast, reducing AR to 0.5 and 0.25 can significantly improve the behavior since only minimal displacement (<0.01D_h) was accumulated after 1000 cycles, exhibiting stable behavior (S). Further reducing Q_{cyc} to 6.7%Q_T resulted in stable behavior for AR = 1.0.

As per Newgard et al. (2015) and Buckley et al. (2023), a power law is employed to fit the displacement accumulation with cycle numbers as per Eq. 6:

$$d_{za}/D_h = \alpha N^{0.8} \quad (6)$$

$$\alpha = max\left[0, (\beta + 0.1 \times Q_{cyc}/Q_t)/\eta\right] \quad (7)$$

$$\beta = -0.014 + 0.0013 \times (AR/AR_{cr})^{3.9} \quad (8)$$

$$\eta = 0.42 + 45 \times 0.07^{(AR/AR_{cr})} \quad 9$$

where d_{za}/D_h is the normalized accumulated displacement, N cycle number, α the power law coefficient, which is a function of Q_{cyc} and AR/AR_{cr}, β and η are fitting parameters related to AR/AR_{cr}, and AR_{cr} the 'critical' AR calculated using Eq. 5. The value of β adjusts the threshold at which displacement will not be accumulated if Q_{cyc}/Q_t is less than this value. The predicted displacements are shown as dashed lines in Figure 8. It shows a globally good fit although a single case (C0.5-1.6) exhibits a considerable overestimation.

Figure 9 presents the displacement accumulation rate Δd_{za}, which is defined in Figure 5. It is interesting to note that for most of the unstable and metastable cases (Figure 9a and b), evolution of Δd_{za} with N can be characterized by two phases. In the first phase, Δd_{za} increased with cycling, followed by the second phase where Δd_{za} tended to decrease to relatively stable values. The reduction of Δd_{za} in the second phase which can last for tens and even a few hundred of cycles is consistent with observations made by other studies on straight-shafted piles (Jardine and Standing 2000) and onshore or smaller diameter screw piles (Hao et al. 2022; Schiavon et al. 2017). The increasing Δd_{za} at the beginning of cycling is similar to an unstable straight-shafted pile prior to failure, indicating a sharp reduction of radial stress on the pile shaft. When assessing the stable cases (Figure 9c), $\Delta d_{za}$is limited and relatively stable throughout cycling as per stable straight-shafted piles.

Evolution of Cyclic Stiffness

The experiments also revealed how cyclic axial loading stiffness k_n (see Figure 5 for definition) evolved with number of cycles. Inspecting the magnitude of loading stiffness (Figure 10b, d and f), it is shown that k_n decreases with increase of Q_{cyc} and lower AR values leads to improved k_n compared with AR = 1.0.

When assessing the evolution of k_n with cycling, similar patterns to those of displacement accumulation rate Δd_{za} (Figure 9) are seen. For the stable cases (Figure 10a and b) k_n shows a trend of stabilization or low-rate reduction. Comparison with model test for straight-shafted piles shows a similar stabilization or reduction with cycle number for stable tests as for the screw piles investigated here (Rimoy et al. 2022; Zheng et al. 2019). In terms of the meta-stable and unstable cases (Figure 10a - f), k_n tends to decrease at the first tens or even hundreds of cycles and then experiences slow recovery. This increase, or recovery, of stiffness is not normally observed for straight-shafted piles. In contrast, the testing of small diameter screw piles by Schiavon et al. (2017) and Hao et al. (2022) (helix/shaft diameter ratios D_h/D_s = 3.3 and 4.0 respectively), showed an initial increase in cyclic stiffness followed by a plateau of constant stiffness. Thus, the general behavior observed in this study with much larger diameter pile shafts (D_h/D_s =1.9) is initially similar to piles relying on

shaft resistance (stable) followed by a recovery phase for the higher magnitude tests (unstable and metastable). This difference in apparent behavior from previous screw pile tests is thought to be due to the geometry of the piles coupled with the cyclic magnitudes. Where the screw piles in this study appear to show some recovery is thought to be associated with reduction in shaft stiffness with mobilization and a greater contribution or mobilization of the helix as this is associated with the tests of high cyclic amplitude that are unstable or metastable (e.g. C0.5-1.92). These observations are consistent with the numerical study of the same pile used herein by Sharif et al. (2021b) who showed that that during a monotonic uplift test, the shaft behaved much stiffer (greater increase of resistance for a given displacement) than the helix before displacement d_z/D_h reached 0.03. Schiavon et al. (2019b) also showed that, subject to cyclic tension, the proportion of loading taken by the helix increased from almost zero to around 60% when Q_{cyc} increased from 10%Q_t to 50%Q_t for the pile geometry investigated in their study (D_h=305 mm, D_s= 101 mm, and H=15 m).

Idealized pile component response and interpretation of overall pile response

As an analogue to end bearing response in compression, the helix bearing response in tension is also typically softer than the shaft friction response, although the shaft resistance tends to reach the ultimate value and be fully mobilized at a lower displacement (Fleming et al. 2009; Schiavon et al. 2019b). Therefore, the shaft component of resistance tends to initially control the overall cyclic pile response at lower cyclic magnitudes as investigated in this study.

Figure 11(a) idealizes the helix and shaft resistance normalized by total resistance against displacement for single cycles. For the stable cases associated with small Q_{cyc}/Q_t, mobilization of both the helix and shaft resistance is limited and limited permanent displacement is accumulated, i.e. a displacement path similar to OAO. In these cases, the limited mobilization of shaft resistance (q_s/Q_s, where Q_s is ultimate shaft resistance) does not induce shaft resistance degradation, as suggested by Jardine and Standing (2012) who indicated that q_s/Q_t less than 50% is unlikely to result in degradation. Therefore, overall cyclic response exhibits a constant limited displacement accumulation rate Δd_{za} (Figure 9c) and constant or moderately declining stiffness k_n (Figure 10a) as per stable straight-shafted piles (Rimoy et al. 2022; Zheng et al. 2019).

When increasing Q_{cyc}/Q_t, more displacement is required to mobilize both the helix and shaft resistance to achieve the target maximum total resistance (q_s+q_h). This may lead to a displacement path of OBC in Figure 11(a), where the shaft resistance is highly mobilized and a permanent displacement of C is accumulated. In this case the high mobilization of shaft resistance (q_s/Q_s) is expected to result in significant degradation of shaft loading stiffness and ultimate resistance. Consequently, an increased permanent displacement is accumulated as per the displacement path CDE. This happens to meta-stable and unstable cases, where the displacement accumulation rate Δd_{za} increases (Figure 9a and b) with

corresponding reduction of loading stiffness k_n (Figure 10c and e) at the beginning of cycling. The significant increase of Δd_{za} and decrease of k_n is similar to the unstable response of a straight-shafted pile prior to failure (Rimoy et al. 2022). However, the displacement accumulation can compress soil above the helix exhibiting a tendency of increasing the local stiffness of helix response as shown in Figure 11(a) where $k_{2h} > k_{1h}$, in line with observations for small screw piles (Schiavon et al. 2017). This increase of helix stiffness can contribute to the increase of overall stiffness (Figure 10c and e) and reduction of displacement accumulation rate Figure 9 after the completion of the shaft resistance degradation at the beginning of cycling.

Over-flighting can also reduce displacement accumulation as illustrated in Figure 11(b). Because of the improved cyclic displacement response due to over-flighting and the stiffer response of shaft resistance, it is assumed that over-flighting contributes an increased proportion of shaft component to the total capacity (Q_s/Q_t) with reduced helix contribution, although the absolute magnitudes of both the helix and shaft resistance components are expected to be improved as discussed previously and suggested by (Sharif et al. 2021a). As shown in Figure 11(b), subject to the same total loading, the improved Q_s/Q_t due to over-flighting allows the stiffer shaft to take an increased load proportion resulting in displacement path being changed from OAB (AR = 1.0) to OA'B' (AR < 1.0) with reduced displacement accumulation, along with reduced load contribution from the softer helix. For lower Q_{cyc}, over-flighting can even result in response modification from unstable (OAB) to stable (OA'B') as shown in Figure 11(c). This corresponds to the stability changing from unstable (C1.0-0.77) to stable (C0.5-0.88 and C0.25-1.03) at Q_{cyc}=13.5%Q_t due to improved shaft resistance with reducing AR.

Post-cyclic Monotonic Response

Another consideration of cyclic screw pile behavior is how the pile capacity evolves with cycling. Figure 12 compares the pre-cyclic and post-cyclic monotonic uplift response. For C1.0-1.6 (Figure 12a), the post-cyclic uplift response appears slightly stiffer than the pre-cyclic response, which is indicated by the increasing cyclic loading stiffness shown in Figure 10(c or e), although the post-cyclic capacity is lower (by 18%). In contrast, the enhanced stiffness was not observed in the rest of cases, which is also indicated by loading stiffness in Figure 10.

Figure 13 shows the relative loss in capacity (ratio of tensile capacity loss $\Delta Q_t = Q_{t\_postcyc} - Q_t$ to pre-cyclic capacity Q_t) that linearly increases with accumulated displacement during cycling and is dependent on installation AR. This linear function is fitted as Eq. 10:

$$\Delta Q_t/Q_t = -2.03 d_{za}/D_h \quad (10)$$

This suggests the potential to predict post-cyclic capacity simply by using accumulated displacement combined with pre-cyclic capacity. In addition, regarding the reduced displacement accumulation as shown in Figure 8, it suggests that over-flighted installation can mitigate capacity degradation caused by cyclic loading.

Although the shaft resistance contributes to the cyclic response as discussed previously, its contribution to the total tensile capacity of the screw pile studied herein was suggested to be less than 20% (Sharif et al. 2021b), the ultimate capacity reduction is therefore predominately associated with the helix. Newgard et al. (2015) suggested that the loss of tensile capacity of a screw pile (or helical plate) due to cyclic loading can be related to loss of helix embedment depth and changes in soil state (e.g. reduction of density). The helix embedment depth and soil parameters are typical inputs for capacity prediction methods of screw piles. For instance, Giampa et al. (2017) proposed a theoretical solution (Eq. 11 ~ 13) to predict tensile capacity of single-helix screw piles with shallow embedment (D_h/H typically below 5 to 12 but this is dependent on relative density) i.e. the failure mechanism can develop to ground surface as an uplifting wedge.

$$\kappa = tan\psi_p + \cos(\varphi_p - \psi_p)(tan\varphi_p - tan\psi_p) \quad (11)$$

$$N_\gamma = 1 + 2\kappa\frac{H}{D_h} + \frac{4}{3}\kappa tan\psi_p\left(\frac{H}{D_h}\right)^2 \quad (12)$$

$$Q_t = \frac{N_\gamma \gamma' H \pi D_h^2}{4} \quad (13)$$

where φ_p is the peak friction angle of the soil, ψ_p is the peak dilation angle of the soil, H is the embedment depth of the helix, D_h is the helix diameter.

This method has been shown to give reasonable prediction of tensile capacity of shallow embedded pitch-matched screw piles (Cerfontaine et al. 2023a; Cerfontaine et al. 2021b) but does not consider installation effects and contribution of shaft resistance (as it is generally considered a minor contribution for onshore screw piles with low shaft diameter D_s and high D_h/D_s ratio that this method has been previously applied to). Figure 14 (a) shows the tensile capacity prediction by Eq. 11 ~ 13 using the soil parameters listed in Table 1 compared to the measured capacities and Figure 14(b) shows the ratio of measured capacity to Giampa et al. (2017) prediction. The Giampa et al. (2017) method gives reasonably good capacity prediction for AR = 1.0 installation with a slight underestimation that is potentially due to ignoring the shaft component.

However, as it cannot capture the changes in the soil created by over-flighting installation (compared to pitch-matched installation), tensile capacity of both AR = 0.5 and 0.25 are significantly underestimated. Based on the measured capacity in this study, the post-installation reference soil parameters (relative density D_{γ_ref}, peak friction angle φ_{p_ref} and dilation angle ψ_{p_ref}) were back-calculated using the Giampa et al. (2017) approach and the relationships between the parameters listed in Table 1.

The back-calculated values are shown in Figure 14(a). They are consistent with an inferred increased density of sand above the helix as a result of over-flighting. Relative density values are derived from peak friction angles for the HST 95 sand based upon the correlations between key parameters and density determined by Al-Defae et al. (2013). The back-calculated results, as shown in Figure 14(a), are obviously shown for indicative or reference purposes as they do not allow for or capture any stress changes around the pile that would occur due to installation.

Figure 15 illustrates the post-cyclic uplift curves, which have been offset by the accumulated displacement during cycling. This means that the displacements of both pre-cyclic and post-cyclic tests are relative to the pile position at the end of installation. The figures also present the peak tensile capacity predicted using the Giampa et al. (2017) approach (Eq. 11 ~ 13), which only considers variation of embedment depth without taking account of the potential change of soil properties during cyclic loading (i.e. the properties for each AR presented in Figure 14a were adopted). The predicted tensile capacities reduce with displacement, i.e. the Giampa et al. (2017) slopes with d_z/D_h, owing to the loss of helix embedment depth (reduction of H in Eq. 11 ~ 13). Compared to the Giampa et al. (2017) capacity predictions where the input parameters are adopted from Figure 14a, the measured post-cyclic capacities are lower. The difference indicates that the soil state changes with strain or displacement accumulation due to cycling are not captured in the Giampa et al. (2017) approach as would be expected and would require further updated input parameters to capture the soil state changes.

Figure 15 also illustrates that the maximum post-cyclic resistance is close to the resistance of the pre-cyclic response at the same offset displacement, and the post-peak behavior reasonably matches the pre-cyclic response. The post-cyclic monotonic response tracking the pre-cyclic monotonic behavior was also observed for end bearing resistance of straight-shaft piles by Galvis-Castro et al. (2023). This indicates that the post-cyclic monotonic uplift behavior is correlated to the pre-cyclic monotonic uplift behavior and the accumulated displacement during cycling. This also indicates that the cyclic loading induced loss of tensile capacity is predominantly due to displacement/strain accumulation and the cyclic loading does not induce significant additional change of soil stress state and density compared to monotonic loading. It also

highlights again that the beneficial effects of installation at varying AR persists during cyclic loading as the pile effectively returns to pre-cyclic monotonic performance.

Cyclic Stability Comparison

Figure 16 shows the cases examined in this study in a cyclic stability diagram, alongside comparison to the zone boundaries proposed by other studies on driven straight shafted piles (Jardine and Standing 2012) and small onshore pitch-matched screw piles (Costa and Costa 2019; Schiavon 2016). The diagram shows improved cyclic stability can be achieved through a reduction in AR, as evidenced by the wider stable zones and narrower unstable zones. Particularly, the low cyclic stability of AR = 1.0 supports the necessity of over-flighting installation for offshore screw piles used as anchors.

Figure 16 also illustrates that reducing AR to 0.25 for the screw pile studied led to similar cyclic stability to ICP field tests conducted on driven straight-shafted piles by Jardine and Standing (2012). However, direct comparisons between the two are not entirely appropriate due to the different mechanisms governing tensile resistance. While the tensile capacity of straight-shafted piles only relies on shaft friction, screw piles benefit from both shaft friction and helix bearing mechanism (Schiavon 2016; Sharif et al. 2021b). Consequently, screw piles have much higher tensile capacity (ultimate resistance) compared to straight-shafted piles with same shaft diameter and length, due to the additional resistance provided by the helix/helices (Al-Baghdadi 2018). For example, in this study and Figure 16 the screw piles experience significantly larger absolute loading than the straight-shafted piles for the same equivalent normalized cyclic loading. For instance, the tensile capacity of an ICP pile with a length of 19 m and shaft diameter of 457 mm was on average 1.5 MN, whereas the tensile capacity Q_t of the 12.8m long screw pile in this study ranged from 5.66 to 7.58 MN (AR = 1.0 to 0.25). The cyclic loading $Q_{cyc} = Q_{mean}$ = 0.88 MN led to a stable behavior of the pile installed at AR = 0.5 (C0.5-0.88), but the ICP straight-shafted pile (Jardine and Standing 2012) would not withstand a single cycle at this magnitude as the maximum loading Q_{max} = 1.76 MN was beyond the tensile capacity Q_t = 1.5 MN. Therefore, although the cyclic stability of the piles in this study appears reduced when compared to Jardine and Standing (2012), they actually can tolerate cyclic loading with much higher absolute values.

When compared to the pitch-matched small diameter onshore screw piles (Costa and Costa 2019; Schiavon 2016), cyclic stability of AR = 1.0 in this study appears reduced. By reducing the AR, any soil degradation during installation above the helix was partially recovered (Sharif et al. 2021a), resulting in comparable cyclic stability to the study by Costa and Costa (2019) in loose sand (D_r < 33%). However, the remarkably good cyclic stability observed by Schiavon (2016) in very dense sand (D_r > 95%) was not attained in this study. This observation suggests a potential relationship that higher soil

relative density may lead to better cyclic stability, but further investigation at a range of relative densities is needed to substantiate this relationship. However, due to the different orders of magnitude of tensile capacity Q_t (less than 0.2 MN for the small diameter onshore screw piles and more than 5 MN for large-sized screw piles tested herein) and the consequently different applications, the comparison of cyclic stability between the offshore and smaller onshore screw piles shown in Figure 16 may not be entirely appropriate and not do justice to the benefit of using much larger screw piles subjected to much greater loading.

Prediction of Post Cyclic Capacity Loss

It is possible to predict the post-cyclic capacity loss versus cycle number *N* and loading amplitude Q_{cyc} by combining the accumulated displacement prediction equations (Eq. 6 ~ 9) and relationship between capacity loss and accumulated displacement (Eq. 10):

$$\Delta Q_t/Q_t = -2.03\alpha N^{0.8} \quad 14$$

where coefficient α is obtained using Eq. 7. The form of equation is similar to the ICP capacity loss prediction approach for straight-shafted piles (Jardine and Standing 2012) and can be re-written as:

$$\Delta Q_t/Q_t = (B + AQ_{cyc}/Q_t) \times N^C \quad 15$$

where the A, B and C are fitting parameters. The values suggested by Jardine and Standing (2012) based on field tests of straight shafted piles and parameters fitted using data in this study for screw piles are shown in Table 3. The form has been modified to include the effects of installation and the values of AR are included for the screw piles.

Based on Eq. 15 and fitting parameters in Table 3 for screw piles, the prediction of capacity loss $\Delta Q_t/Q_t$ against applied cyclic amplitude Q_{cyc}/Q_t at certain cycle numbers (N = 10, 100 and 100) and at AR =0.5 are shown in Figure 17, with a comparison to ICP capacity loss prediction for straight-shafted piles (Jardine and Standing 2012). As per Jardine and Standing (2012) the lines are constructed based upon:

$$Q_{t\_postcyc} = 1 + \Delta Q_t/Q_t > Q_{max} = Q_{mean} + Q_{cyc} \quad 16$$

which requires the $Q_{t\_postcyc}$ to remain higher than applied Q_{max}. Figure 17 indicates that the form of screw pile capacity degradation adopted is appropriate when compared to the ICP approach used for straight-shafted piles.

Limitations and Practical Implications

This study makes a first step towards understanding the effects of installation on the cyclic performance of large screw piles deployed as anchors for floating wind and paves the way for further studies. It is noted though that the centrifuge tests presented in this paper are limited to installation and tensile cyclic loading regimes of a single screw pile in specific ground conditions (medium dense sand). In addition, it is acknowledged that the study here has adopted fully drained installation and loading cases under simple cyclic loading scenarios. This may not reflect the complexity of a particular deployment that would require site specific assessment of ground conditions, drainage regimes and cyclic pore pressure accumulation effects and consider loading events such as snatch loading and storm build up events. That said though, such site-specific studies can easily be incorporated in further centrifuge testing or centrifuge testing included as part of the design process as suggested in ISO 19901-4:2016 (International Organization for Standardization 2016).

However, there are important practical implications for screw piles deployment for further floating wind anchorage. Firstly, this paper has shown that the over-flighting during installation, which may be necessary for large-sized screw piles (Davidson et al. 2022), is also beneficial for cyclic tensile loading regimes. Based upon this study and for the pile investigated herein an AR = 0.25 is associated with optimal behavior. For practical application, installation rigs would then need to be developed that have control on both rotational rate as well as penetration rate and have the ability to apply both tensile and compressive forces to the pile. It may be more ideal in an offshore setting to develop pile designs that allow optimal installation under self-weight penetration to avoid the need for heavy rigs required to create reaction to installation. Further characterization of the performance of piles installed in this manner would be required.

As previously discussed, the cyclic tensile response under loading regimes considered in this study is more controlled by the shaft resistance, and the over-flighting induced improvement on cyclic tensile response relates to the enhanced shaft resistance component as previously observed for monotonically loaded piles (Sharif et al. 2021a). In addition, the mobilization of the helix resistance is likely to be accompanied with high cyclic displacement accumulation rates due to the lower loading stiffness of the helix bearing mechanism. Therefore, for design where lower magnitude cyclic loading regimes are considered, the helix resistance may need to be ignored for cyclic checks and the pile treated as a straight-shafted pile. In this case, the helix is predominantly employed to allow the silent rotary installation and deal with large storm events and snatch loading events.

This study also presents a method for predicting accumulated displacement and capacity loss due to cyclic loading, taking account of the effect of varying AR. This method can be used for initial cyclic design and pile sizing. In addition,

comparison between the proposed screw pile accumulated displacement and capacity loss prediction method and those previously developed for straight-shafted piles shows that over-flighted screw piles exhibit similar overall cyclic stability to straight-shafted piles. Due to the higher monotonic capacity, screw piles can take higher cyclic loading than straight-shafted piles with same shaft diameter. Therefore, replacing straight-shafted piles with over-flighted screw piles could be an attractive solution for anchoring floating renewable energy structures.

Conclusion

A series of centrifuge tests were conducted to investigate the over-flighting effects on cyclic performance of a single-helix offshore screw pile. Over-flighting (AR<1) during installation has been shown to improve the monotonic uplift response of upscaled screw piles for offshore energy applications. The pile was installed at advancement ratios, AR = 1.0, 0.5 and 0.25, which caused compressive, nearly net zero and tensile force, respectively, on the pile head during installation. The cyclic loading amplitudes, Q_{cyc} were varied from 6.7% to 28.6% Q_t. Post-cyclic monotonic uplift tests were conducted on each pile to evaluate the effects of cyclic loading on the final post-cyclic tensile capacity. The main conclusions are as follows:

a) It is possible to reduce uplift displacement accumulation by reducing AR during installation (over-flighting). For the offshore screw pile investigated, considering ultimate displacement as 10%D_h, it could not tolerate more than 100 cycles when subject to cyclic loading if the installation of pile followed a pitch-matched approach (AR = 1.0). However, when subjected to the same cyclic loading magnitude, the piles installed at AR = 0.5 and 0.25 could accommodate more than hundreds and even thousands of cycles exhibiting meta-stable or stable behavior.

b) Compared to pitch-matched installation, screw piles installed at lower AR values exhibited higher cyclic loading stiffness, k_n.

c) For stable cases associated with lower Q_{cyc}, the pile is assumed to behave similarly to a straight-shafted pile and exhibits decreased or stable loading stiffness k_n with cycling. Larger Q_{cyc} leads to meta-stable and unstable response accompanied by degradation of shaft resistance and mobilization of helix resistance. The degradation of shaft resistance leads to an increased displacement accumulation rate (Δd_{za}) and decreased k_n within the first tens or hundreds of cycles, and the Δd_{za} tends to decrease or become stable and k_n tends to increase with the mobilization of helix resistance in further cycles.

d) When displacement accumulation is low to moderate (<0.11D_h in this study), post-cyclic monotonic uplift response returns to the pre-cyclic monotonic uplift response when compared at the same accumulated

displacement level. This suggests that reduction of tensile capacity is predominately due to the displacement accumulation itself and the effect of loading history difference (monotonic or cyclic) is limited.

e) Reducing the value of AR has been shown to give comparable cyclic stability performance to straight shafted piles and screw piles investigated in previous studies even where the screw piles tested herein have been tested to much greater load magnitudes.

f) Prediction frameworks for displacement accumulation and capacity loss were developed considering the effect of AR values adopted for installation. The predictions show that the over-flighted screw piles, e.g. AR = 0.5 herein, would experience similar capacity degradation to straight-shafted piles.

Data Availability Statement

All data that support the findings of this study are available from the corresponding author upon reasonable request.

Acknowledgements

The first author would like to acknowledge the financial support from Chinese Scholarship Council (CSC) and the University of Dundee.

Notation List

The following symbols are used in this paper:

AR = advancement ratio

D_h = pile helix diameter

D_r = soil relative density

D_{r_ref} = soil reference relative density

D_s = pile shaft diameter

d_z = pile uplift displacement

d_{za} = accumulated pile uplift displacement

d_{50} = mean diameter of sand grains

g_d = centrifuge acceleration in a dry sand test

g_{sat} = centrifuge acceleration in a saturated sand test

H = helix embedment depth

k_n = loading stiffness in cycle N

k_1 = loading stiffness in the first cycle

L = pile length

N = loading cycle number

p_h = helix geometric pitch

Q_{cyc} = cyclic loading amplitude

Q_{max} = maximum tensile force in a loading cycle

Q_{mean} = mean value of cyclic loading

572 Q_{min} = minimum tensile force in a loading cycle

573 Q_s = tensile capacity of pile shaft

574 Q_t = tensile capacity of pile

575 $Q_{t\_postcyc}$ = post-cyclic tensile capacity of pile

576 q_h = mobilized helix resistance

577 q_s = mobilized shaft resistance

578 z = soil depth

579 ρ_d = dry soil density

580 ρ' = buoyant density of saturated soil

581 ${\sigma_p}'$ = mean soil effective stress

582 ${\sigma_v}'$ = vertical component of soil effective stress

583 φ_p = soil peak friction angle

584 φ_{p_ref} = soil reference peak friction angle

585 ψ_p = soil peak dilation angle

586 ψ_{p_ref} = soil reference peak dilation angle

587 Δd_{za} = uplift displacement accumulation rate

588 ΔQ_t = difference of tensile capacity of piles before Q_t and after $Q_{t\_postcyc}$ cyclic loading

589 Δ_z = vertical displacement per rotation during installation

590 **References**

591 Al-Baghdadi, T. (2018). "Screw piles as offshore foundations: Numerical and physical modelling." Ph.D Thesis, University
592 of Dundee, UK.
593 Al-Defae, A. H., Caucis, K., and Knappett, J. A. (2013). "Aftershocks and the whole-life seismic performance of granular
594 slopes." *Geotechnique*, 63(14), 1230-1244.

Bolton, M. D., Gui, M. W., Garnier, J., Corte, J. F., Bagge, G., Laue, J., and Renzi, R. (1999). "Centrifuge cone penetration tests in sand." *Geotechnique*, 49(4), 543-552.
British Standards Institution (2015). "BS8004: Code of practice for foundations." BSI, London, UK.
Buckley, R. M., Jardine, R. J., Kontoe, S., Liu, T., Byrne, B. W., McAdam, R. A., Schranz, F., and Vinck, K. (2023). "Axial cyclic loading of piles in low-to-medium-density chalk." *Géotechnique*, 1-14.
Cerato, A. B., and Victor, R. (2014). "Effects of helical anchor geometry on long-term performance of small wind tower foundations subject to dynamic loads." *DFI Journal - The Journal of the Deep Foundations Institute*, 2(1), 30-41.
Cerfontaine, B., Brown, M. J., Davidson, C., Sharif, Y. U., Huisman, M., and Ottolini, M. (2022). "Optimised screw pile design for offshore jacket foundations in medium–dense sand." *Géotechnique Letters*, 12(2), 114-119.
Cerfontaine, B., Brown, M. J., Knappett, J. A., Davidson, C., Sharif, Y. U., Huisman, M., Ottolini, M., and Ball, J. D. (2023a). "Control of screw pile installation to optimise performance for offshore energy applications." *Géotechnique*, 73(3), 234-249.
Cerfontaine, B., Ciantia, M. O., Brown, M. J., and Sharif, Y. U. (2021a). "DEM study of particle scale and penetration rate on the installation mechanisms of screw piles in sand." *Computers and Geotechnics*, 139.
Cerfontaine, B., Knappett, J. A., Brown, M. J., and Bradshaw, A. S. (2019). "Effect of soil deformability on the failure mechanism of shallow plate or screw anchors in sand." *Computers and Geotechnics*, 109, 34-45.
Cerfontaine, B., Knappett, J. A., Brown, M. J., Davidson, C. S., Al-Baghdadi, T., Sharif, Y. U., Brennan, A., Augarde, C., Coombs, W. M., Wang, L., Blake, A., Richards, D. J., and Ball, J. (2021b). "A finite element approach for determining the full load–displacement relationship of axially loaded shallow screw anchors, incorporating installation effects." *Canadian Geotechnical Journal*, 58(4), 565-582.
Cerfontaine, B., White, D., Kwa, K., Gourvenec, S., Knappett, J., and Brown, M. (2023b). "Anchor geotechnics for floating offshore wind: Current technologies and future innovations." *Ocean Engineering*, 279.
Costa, P. d. S. J., and Costa, D. J. Y. (2019). "Cyclic stability of helical anchors installed in a sedimentary sand deposit." *Proceedings of the XVI Pan-American Conference on Soil Mechanics and Geotechnical Engineering*, P. L.-A. Norma, M.-H. Eduardo, L. E.-S. Alejandra, M.-P. José Alfredo, and O. L. Alexandra, eds., IOS Press, Cancun, Mexico.
Davidson, C., Al-Baghdadi, T., Brown, M. J., Knappett, J., Brennan, A. J., and Augarde, C. E. (2018). "Centrifuge modelling of screw piles for offshore wind energy foundations." *Physical Modelling in Geotechnics: Proceedings of the 9th International Conference on Physical Modelling in Geotechnics*, S. Mcnamara, S. Divall, and R. Goodey, eds., Taylor & Francis, London, United Kingdom, 695-700.
Davidson, C., Brown, M., Cerfontaine, B., Al-Baghdadi, T., Knappett, J., Brennan, A. J., Augarde, C., Coombs, W. M., Wang, L., Blake, A., Richards, D., and Ball, J. (2022). "Physical modelling to demonstrate the feasibility of screw piles for offshore jacket-supported wind energy structures." *Geotechnique*, 72(2), 108-126.
Ding, H., Wang, L., Zhang, P., Liang, Y., Tian, Y., and Qi, X. (2019). "The recycling torque of a single-plate helical pile for offshore wind turbines in dense sand." *Applied Sciences*, 9(19).
Fleming, K., Weltman, A., Randolph, M., and Elson, K. (2009). *Piling engineering*, Taylor & Francis, London, UK.
Galvis-Castro, A. C., Tovar-Valencia, R. D., Prezzi, M., and Salgado, R. (2023). "Effect of cyclic loading on the mobilization of unit base resistance of model piles jacked in sand." *Acta Geotechnica*.
Garnier, J., Gaudin, C., Springman, S. M., Culligan, P. J., Goodings, D., Konig, D., Kutter, B., Phillips, R., Randolph, M. F., and Thorel, L. (2007). "Catalogue of scaling laws and similitude questions in geotechnical centrifuge modelling." *International Journal of Physical Modelling in Geotechnics*, 7(3), 1-23.
Giampa, J. R., Bradshaw, A. S., and Schneider, J. A. (2017). "Influence of Dilation Angle on Drained Shallow Circular Anchor Uplift Capacity." *International Journal of Geomechanics*, 17(2).
Hao, D., Che, J., Chen, R., Zhang, X., Yuan, C., and Chen, X. (2022). "Experimental investigation on behavior of single-helix anchor in sand subjected to uplift cyclic loading." *Journal of Marine Science and Engineering*, 10(10).
Hao, D. X., Wang, D., O'Loughlin, C. D., and Gaudin, C. (2019). "Tensile monotonic capacity of helical anchors in sand: interaction between helices." *Canadian Geotechnical Journal*, 56(10), 1534-1543.
Herbert-Read, J. E., Kremer, L., Bruintjes, R., Radford, A. N., and Ioannou, C. C. (2017). "Anthropogenic noise pollution from pile-driving disrupts the structure and dynamics of fish shoals." *Proceedings of the Royal Society B - Biological Sciences*, 284(1863).
International Organization for Standardization (2016). "ISO 19901-4:2016 Petroleum and natural gas industries — Specific requirements for offshore Structures Part 4: Geotechnical and foundation design considerations." International Organization for Standardization.
Jardine, R. J., and Standing, J. R. (2000). "Pile load testing performed for HSE cyclic loading study at Dunkirk, France." Health and Safety Executive, London.
Jardine, R. J., and Standing, J. R. (2012). "Field axial cyclic loading experiments on piles driven in sand." *Soils and Foundations*, 52(4), 723-736.
Klinkvort, R. T., and Hededal, O. (2013). "Lateral response of monopile supporting an offshore wind turbine." *Proceedings of the Institution of Civil Engineers - Geotechnical Engineering*, 166(2), 147-158.

Ko, H.-Y., Atkinson, R. H., Goble, G. G., and Ealy, C. D. (1984). "Centrifugal modeling of pile foundations." *Analysis and Design of Pile Foundations*, J. R. Meyer, ed., ASCE, San Francisco, California, USA, 21-40.
Lauder, K. (2010). "The performance of pipeline ploughs." Ph.D Thesis, University of Dundee, UK.
Le Kouby, A., Canou, J., and Dupla, J. C. (2004). "Behaviour of model piles subjected to cyclic axial loading." *International Conference on cyclic behaviour of soils and liquefaction phenomena*, T. Triantafyllidis, ed., A. A. Balkema, Leiden, Bochum, 159-166.
Li, Z., Haigh, S. K., and Bolton, M. D. (2010). "Centrifuge modelling of mono-pile under cyclic lateral loads." *Physical Modelling in Geotechnics - Proceedings of the 7th International Conference on Physical Modelling in Geotechnics (ICPMG 2010)*, S. Springman, J. Laue, and L. Seward, eds., CRC Press, Zurich, Switzerland, 965-970.
Lutenegger, A. J. (2011). "Behavior of Multi-Helix Screw Anchors in Sand." *14th Pan-American Conference on Soil Mechanics and Geotechnical Engineering*, Canadian Geotechnical Society, Toronto, Ontario, Canada.
Mortara, G., Mangiola, A., and Ghionna, V. N. (2004). "Cyclic behaviour of sand-structure interfaces." *International Conference on cyclic behaviour of soils and liquefaction phenomena*, T. Triantafyllidis, ed., A. A. Balkema, Leiden, Bochum, 173-178.
Mortara, G., Mangiola, A., and Ghionna, V. N. (2007). "Cyclic shear stress degradation and post-cyclic behaviour from sand–steel interface direct shear tests." *Canadian Geotechnical Journal*, 44(7), 739-752.
Newgard, J. T., Schneider, J. A., and Thompson, D. (2015). "Cyclic response of shallow helical anchors in a medium dense sand." *3rd Conference on Frontiers in Offshore Geotechnics*, V. Meyer, ed., Taylor & Francis, Oslo, Norway, 913-918.
Perko, H. (2009). *Helical Piles A Practical Guide to Design and Installation*, John Wiley & Sons, New Jersey, US.
Poulos, H. G. (1989). "Cyclic axial loading analysis of piles in sand." *Journal of Geotechnical Engineering-ASCE*, 115(6), 836-852.
Puech, A., and Garnier, J. (2017). *Design of Piles under Cyclic Loading*, John Wiley & Sons., London, UK.
Rafsanjani, A. A. H., Salehzadeh, H., and Nuri, H. (2021). "Evaluating scale effects and bearing portions in centrifuge modeling of helical anchors: sand." *Acta Geotechnica*, 16, 2917-2932.
Rimoy, S., Silva I, M., and Jardine, R. J. (2022). "Stability and load-displacement behaviour of axially cyclic loaded displacement piles in sands." *Canadian Geotechnical Journal*, 59(8), 1358-1372.
Schiavon, A. J. (2016). "Behaviour of helical anchors subjected to cyclic loadings."Ph.D Thesis, Universidade de São Paulo, Brazil.
Schiavon, J. A., Tsuha, C. d. H. C., Neel, A., and Thorel, L. (2019a). "Centrifuge modelling of a helical anchor under different cyclic loading conditions in sand." *International Journal of Physical Modelling in Geotechnics*, 19(2), 72-88.
Schiavon, J. A., Tsuha, C. d. H. C., and Thorel, L. (2016). "Scale effect in centrifuge tests of helical anchors in sand." *International Journal of Physical Modelling in Geotechnics*, 16(4), 185-196.
Schiavon, J. A., Tsuha, C. d. H. C., and Thorel, L. (2019b). "Monotonic, cyclic and post-cyclic performances of single-helix anchor in residual soil of sandstone." *Journal of Rock Mechanics and Geotechnical Engineering*, 11(4), 824-836.
Schiavon, J. A., Tsuha, C. H. C., and Thorel, L. (2017). "Cyclic and post-cyclic monotonic response of a single-helix anchor in sand." *Géotechnique Letters*, 7(1), 11-17.
Sharif, Y. U., Brown, M. J., Cerfontaine, B., Davidson, C., Ciantia, M. O., Knappett, J. A., Ball, J. D., Brennan, A., Augarde, C., Coombs, W., Blake, A., Richards, D., White, D., Huisman, M., and Ottolini, M. (2021a). "Effects of screw pile installation on installation requirements and in-service performance using the discrete element method." *Canadian Geotechnical Journal*, 58(9), 1334-1350.
Sharif, Y. U., Brown, M. J., Ciantia, M. O., Cerfontaine, B., Davidson, C., Knappett, J. A., and Ball, J. (2021b). "Assessing single-helix screw pile geometry on offshore installation and axial capacity." *Proceedings of the Institution of Civil Engineers - Geotechnical Engineering*, 174(5), 512-529.
Spagnoli, G., and Tsuha, C. (2020). "A review on the behavior of helical piles as a potential offshore foundation system." *Marine Georesources & Geotechnology*, 38(9), 1013-1036.
Ueno, K. (1998). "Methods for preparation of sand sample." *Centrifuge 98*, T. Kimura, and J. Takemura, eds., Balkema, Tokyo, Japan, 1047-1055.
Ullah, S. N., O'Loughlin, C., Hu, Y., and Hou, L. F. (2023). "Torsional installation and vertical tensile capacity of helical piles in clay." *Géotechnique*, 1-17.
Viggiani, C. (1989). "Influenza dei fattori tecnologici sul comportamento dei pali." *Atti, XVII Convegno Nazionale di Geotecnica*Taormina, 83–91.
Wang, W., Brown, M. J., Ciantia, M. O., and Sharif, Y. U. (2021). "DEM simulation of cyclic tests on an offshore screw pile for floating wind." *18th UK Travelling Workshop: GeoMechanics: from Micro to Macro (GM3)*, M. Ciantia, M. Previtali, and M. Bolton, eds., University of Dundee, Dundee, UK, 29-32.
Wang, W., Brown, M. J., Ciantia, M. O., Sharif, Y. U., and Cerfontaine, B. (2023a). "DEM analysis of helix number effects on offshore screw pile installation and in-service performance." *10th European Conference on Numerical Methods in Geotechnical Engineering* L. Zdravković, S. Konte, D. M. G. Taborda, and A. Tsiampousi, eds.London, UK.
Wang, W., Brown, M. J., Sharif, Y. U., and Davidson, C. (2023b). "The influence of the installation advancement ratio on the cyclic performance of a single-helix pile for floating offshore wind applications." *9th International SUT OSIG*

712 *Conference - Innovative Geotechnologies for Energy Transition*, Society for Underwater Technology, London, UK,
713 1218-1224.
714 Zhang, Z., and Wang, Y.-H. (2015). "Three-dimensional DEM simulations of monotonic jacking in sand." *Granular*
715 *Matter*, 17(3), 359-376.
716 Zheng, B. L., Kutter, B. L., Wilson, D. W., Allmond, J., Hunt, C., and McNeilan, T. (2019). "Centrifuge Modeling of
717 Cyclic Degradation of Axially Loaded Piles in Sand for Offshore Wind Turbine Structures." *International Journal of*
718 *Offshore and Polar Engineering*, 29(2), 172-181.
719

720 **Table**

721 *Table 1 Properties of the HST95 sand (after Al-Defae et al. (2013))*

Properties	Symbol	Value	Value of D_r = 50%
Effective particle size [mm]	d_{10}	0.090	-
Mean particle size [mm]	d_{50}	0.141	-
Particle specific gravity [-]	G_s	2.63	-
Minimum void ratio [-]	e_{min}	0.467	-
Maximum void ratio [-]	e_{max}	0.769	-
Dry unit weight [kg/m^3]	γ_{dry}	14.5+3×D_r	16.0
Saturated unit weight [kg/m^3]	γ_{sat}	18.8+1.8×D_r	19.7
Critical state friction angle [°]	φ_c	32	-
Peak friction angle [°]	φ_p	29+20×D_r	39.0
Peak dilation angle [°]	ψ_p	-4.4+26×D_r	8.6
Steel-sand interface friction angle [°]	δ	24	-

722

723

724 *Table 2 Summary of tests conducted*

Test ID	**AR**	**Loading regime**	**Cycle number, N**	d_{za}/D_h	Q_t **(MN)**	$Q_{t\_postcyc}$ **(MN)**	**Stability**
M1.0	1.0	Monotonic uplift	-	-	5.66	-	-
M0.5	0.5	Monotonic uplift	-	-	6.79	-	-
M0.25	0.25	Monotonic uplift	-	-	7.58	-	-
C1.0-1.6	1.0	$Q_{cyc} = Q_{mean}$ = 1.6 MN (28.6%Q_t)	8	0.09	-	4.61	US
C0.5-1.6	0.5	$Q_{cyc} = Q_{mean}$ = 1.6 MN (23.8%Q_t)	500	0.1	-	5.48	MS
C0.25-1.6	0.25	$Q_{cyc} = Q_{mean}$ = 1.6 MN (21.2%Q_t)	900	0.1	-	6.38	MS
C0.5-1.92	0.5	$Q_{cyc} = Q_{mean}$ = 1.92 MN (28.6%Q_t)	88	0.11	-	5.37	US
C0.25-2.17	0.25	$Q_{cyc} = Q_{mean}$ = 2.17 MN (28.6%Q_t)	400	0.1	-	6.35	MS
C1.0-0.77	1.0	$Q_{cyc} = Q_{mean}$ = 0.77 MN (13.5% Q_t)	120	0.4	-	0.94	US
C0.5-0.88	0.5	$Q_{cyc} = Q_{mean}$ = 0.88 MN (13.5% Q_t)	1000	-0.002	-	6.98	S
C0.25-1.03	0.25	$Q_{cyc} = Q_{mean}$ = 1.03 MN (13.5% Q_t)	1000	-0.009	-	7.35	S
C1.0-0.39	0.25	$Q_{cyc} = Q_{mean}$ = 0.39 MN (6.7% Q_t)	1000	0.006	-	5.53	S

725

726

727 *Table 3 Fitting parameters for cyclic capacity degradation: ICP straight-shafted piles and screw piles in this study*

Datasets	**A**	**B**	**C**
Jardine and Standing (2012)	-0.126	0.0126	0.45
Screw piles (this study)	$\frac{-0.2}{0.42+45\times 0.07^{\mathrm{AR}/\mathrm{AR}_{cr}}}$	$0.14+0.013\times(\mathrm{AR}/\mathrm{AR}_{cr})^{3.9}$	0.8

728

729

Figure caption

Figure 1 Schematic showing idealization of screw pile installation effects on in-situ soil conditions (a) pitch-matched and (b) over-flighting (not to scale)

Figure 2 Screw pile model (a) whole pile model; (b) local detail of the helix region (prototype dimensions in brackets)

Figure 3 Typical testing procedure in a single centrifuge test: (a) monotonic test on a pile (b) cyclic and post-cyclic monotonic test on a pile (installation at AR = 0.25)

Figure 4 Definition of cyclic loading parameters

Figure 5 Schematic illustration of cyclic displacement and stiffness parameters

Figure 6 Installation requirements with varying advancement ratio (AR) (a) vertical force and (b) torque

Figure 7 Comparison of the monotonic uplift response of the screw pile installed at different AR

Figure 8 Comparison of normalized accumulated uplift displacement d_{za}/D_h during cyclic loading with varying AR: measurements and predictions from Eq. 6: (a) Q_{cyc} = 1.6 MN; (b) Q_{cyc} = 28.6%Q_t; (c) Q_{cyc} < 13.5%Q_t (US, MS and S refer to unstable, metastable and stable respectively as defined previously)

Figure 9 Comparison of displacement accumulation rate Δd_{za} with varying AR and Q_{cyc}: (a) unstable cases (b) meta-stable cases; (c) stable cases

Figure 10 Effect of AR on cyclic loading stiffness: (a) k_n/k_1 and (b) k_n for $Q_{cyc} \leqslant$ 13.5%Q_t; (c) k_n/k_1 and (d) k_n for Q_{cyc} = 1.6 MN; (e) k_n/k_1 and (f) k_n for Q_{cyc} = 28.6%Q_t

Figure 11 Idealized helix and shaft cyclic force-displacement response of a screw pile (a) a stable cycle subject to a lower loading amplitude and two unstable (or meta-stable) cycles subject to a higher loading amplitude; (b) reduced displacement accumulation in an unstable (or metastable) cycle with over-flighting; (c) transition from an unstable to a stable cycle by over-flighting (ultimate helix resistance is not presented as its value is out of the y-axis range)

Figure 12 Monotonic uplift reponse after (post) cyclic loading regimes with comparison to pre-cyclic monotonic uplift reponse (a) AR = 1.0, (b) AR = 0.5, (c) AR = 0.25

Figure 13 Relationship between apparent cyclic loss in capacity and displacement accumulated during cycling

Figure 14 (a) Pre-cyclic tensile capacity of varying AR values compared to Giampa et al. (2017) prediction and reference soil parameters back calculated using the Giampa et al. (2017) approach (b) ratios of measured capacity to predictions

Figure 15 Displacement corrected post-cyclic monotonic uplift reponse with comparison to pre-cyclic monotonic uplift reponse and Giampa et al. (2017) capacity predictions (a) AR = 1.0, (b) AR = 0.5, (c) AR = 0.25

Figure 16 Cyclic stability diagram with comparison to previous studies of both straight shafted piles (Jardine and Standing 2012) and screw piles (Costa and Costa 2019; Schiavon 2016) (datapoints slightly offset for clarity)

Figure 17 Capacity based interaction diagram. Comparison between experimental data and predictions by Eq. 16 using parameters calibrated in this study and the ICP Dunkirk tests (Jardine and Standing 2012) (a) AR = 0.5 (b) AR = 0.25

Figure

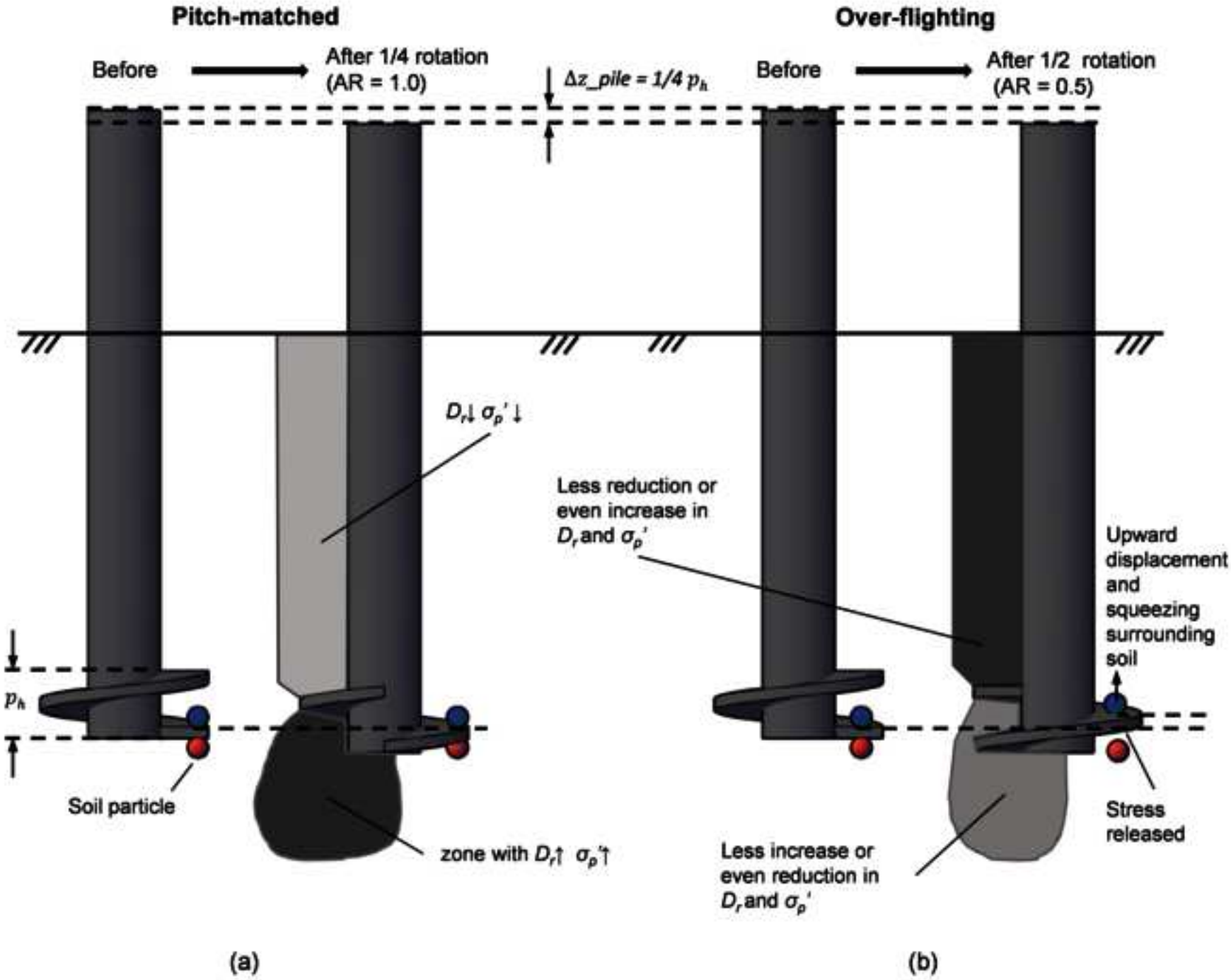

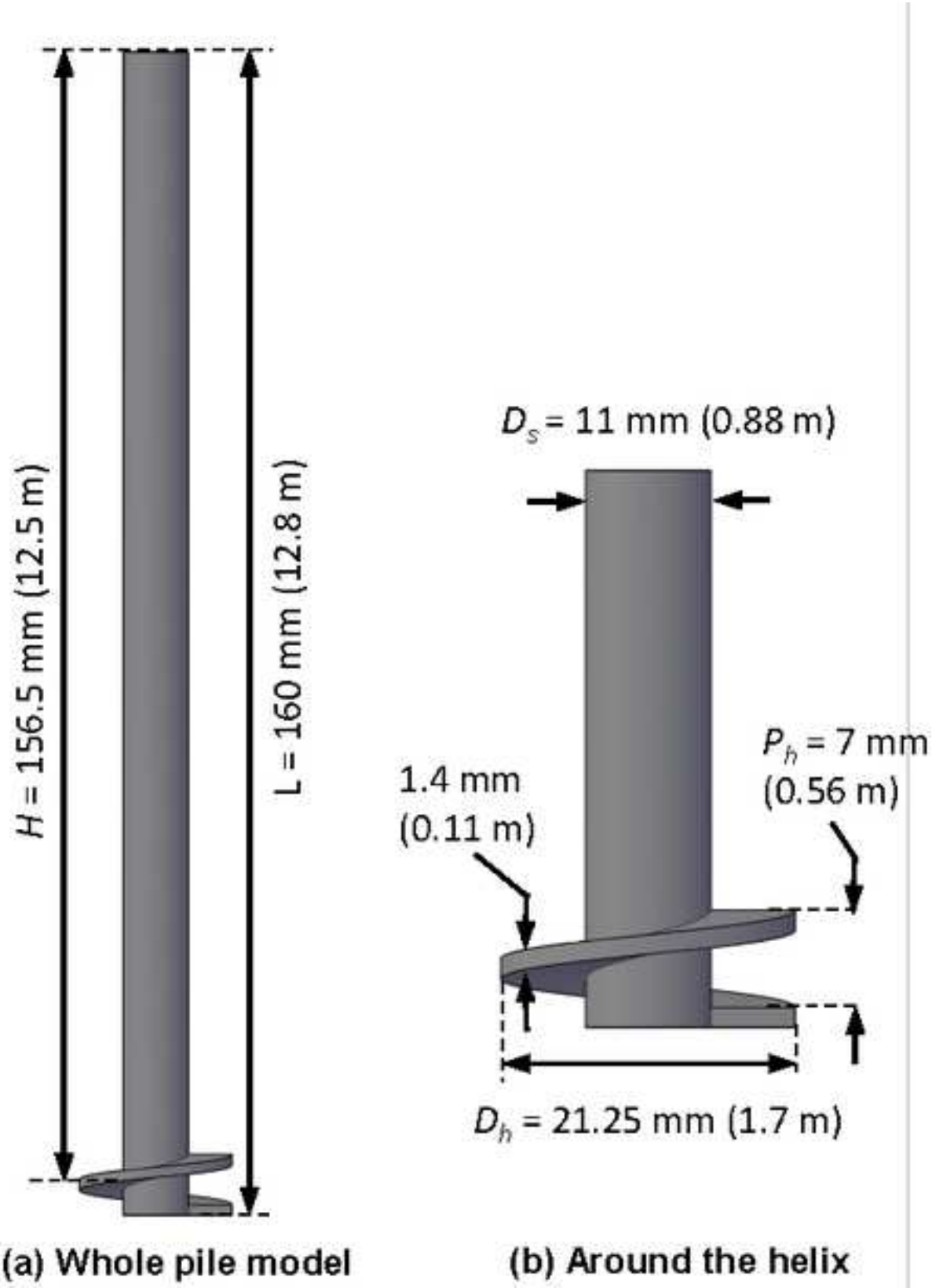

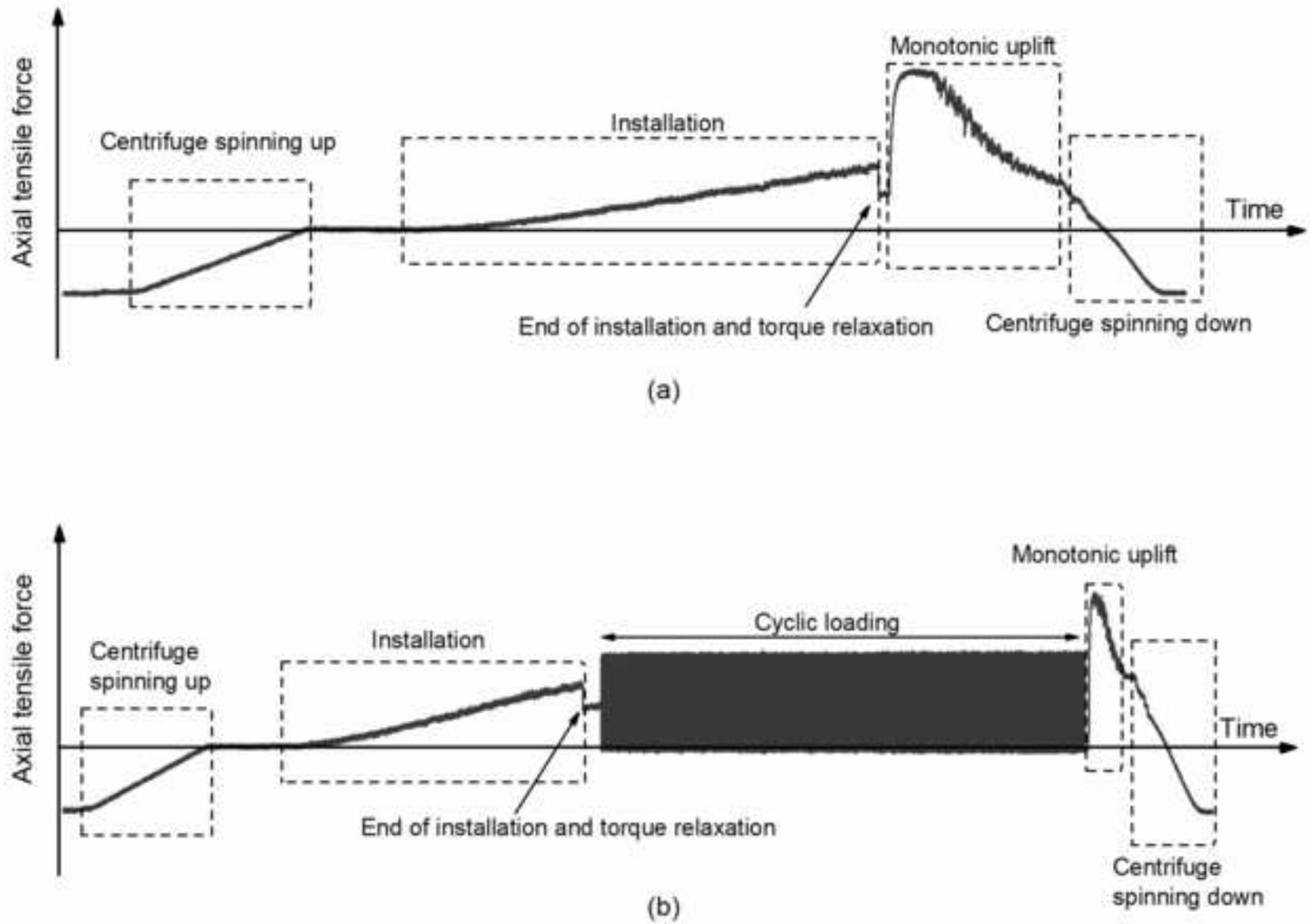

fig 4

Click here to access/download;Figure;Fig 4.tif

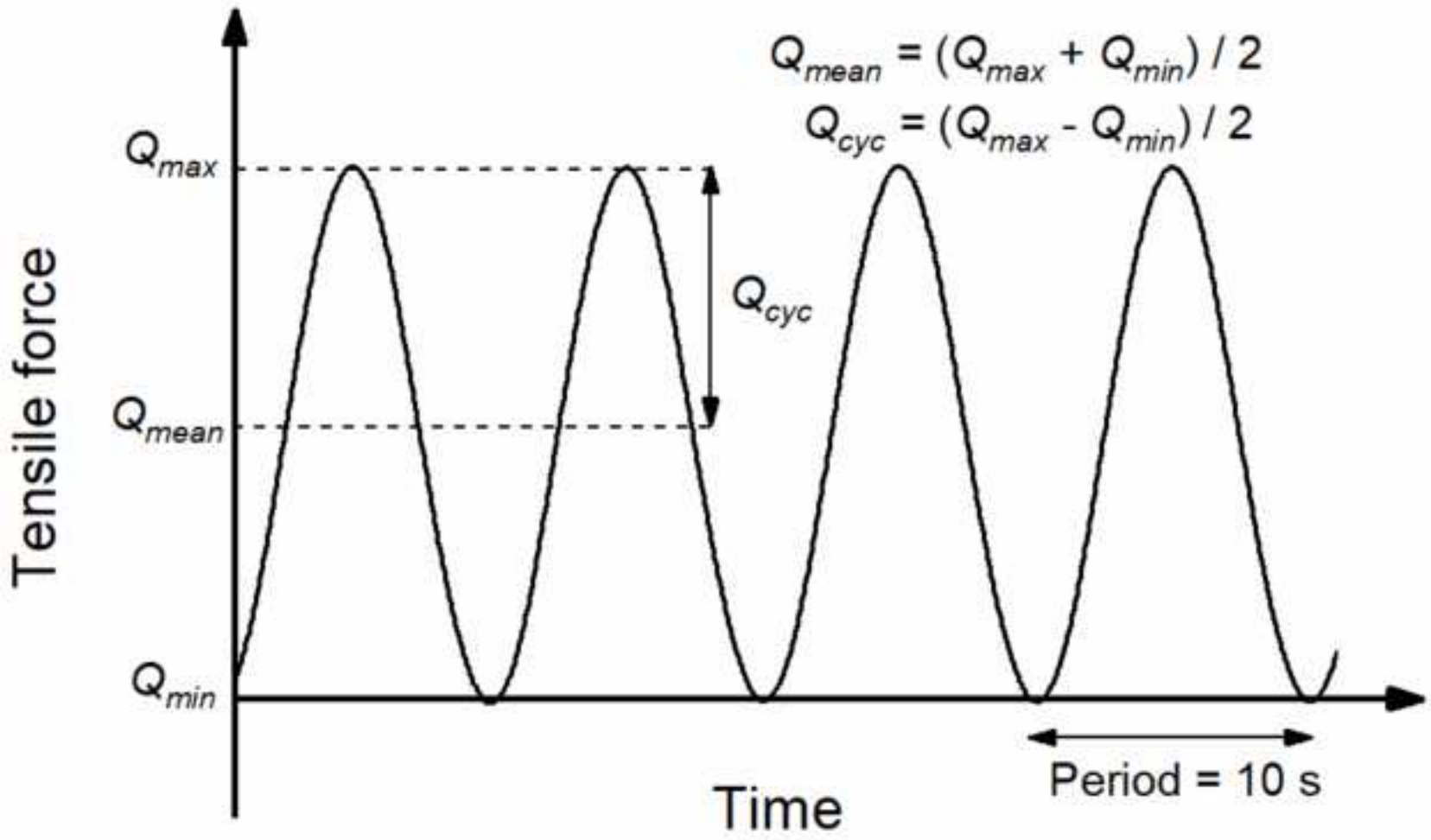

fig 5

Click here to access/download;Figure;Fig 5.tif

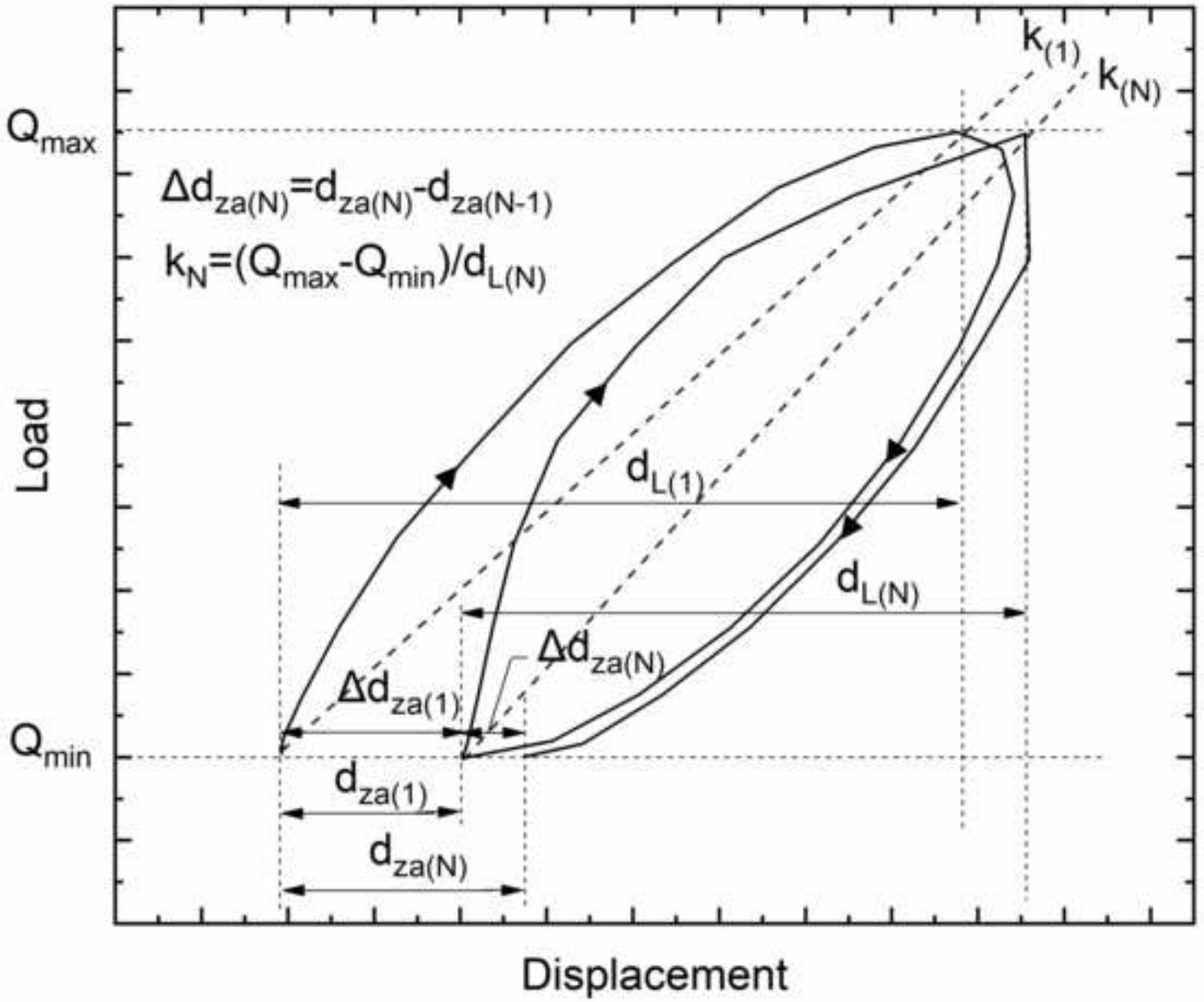

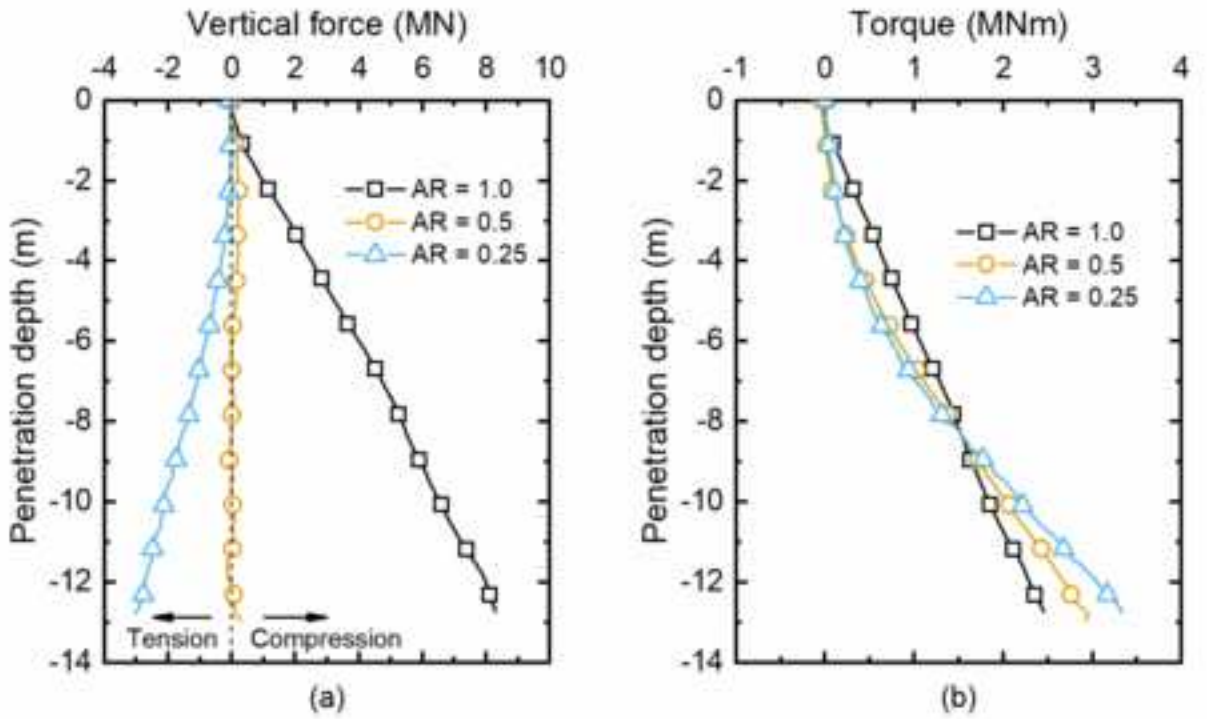

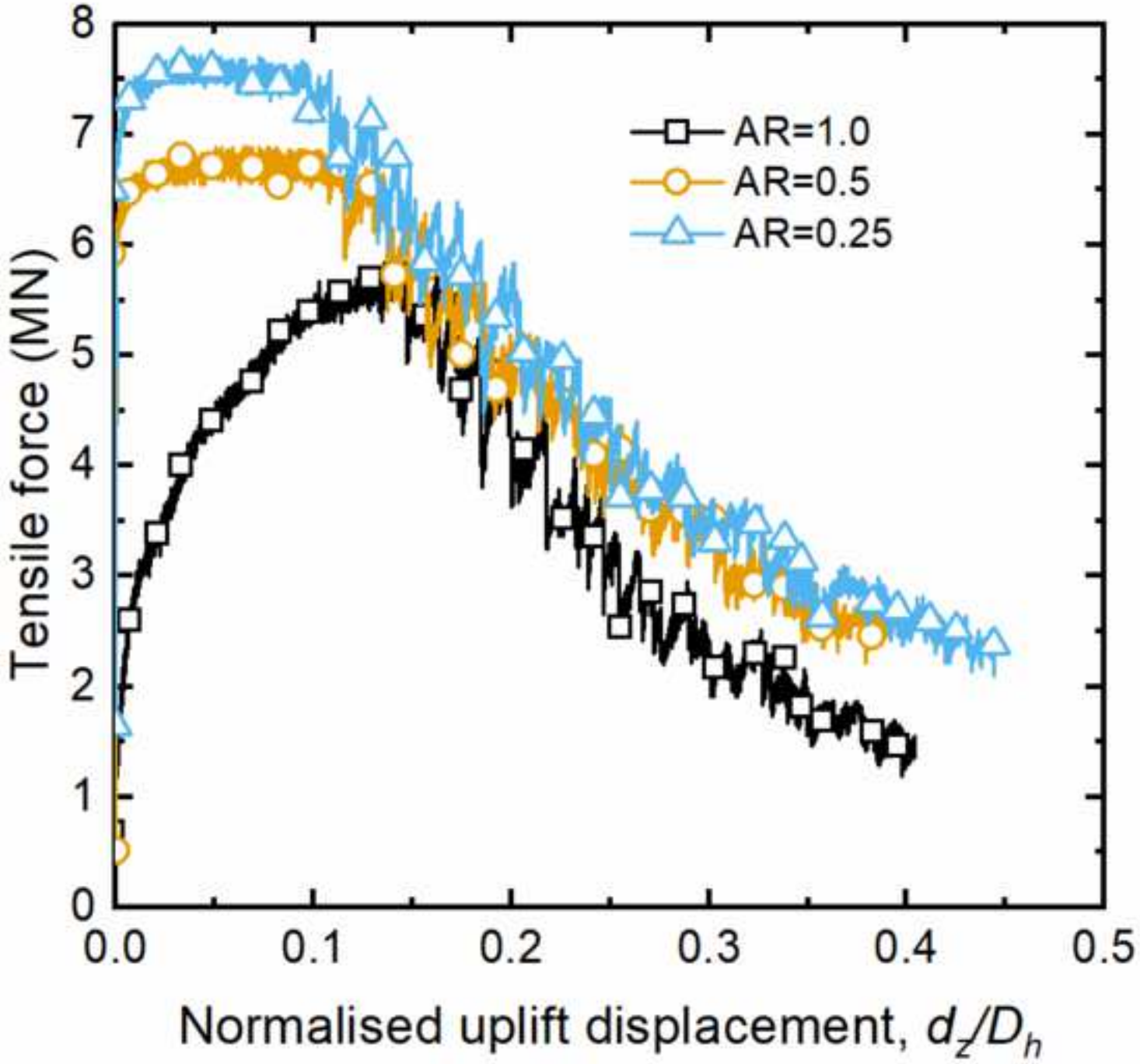

fig 8

Click here to access/download;Figure;fig 8.tif

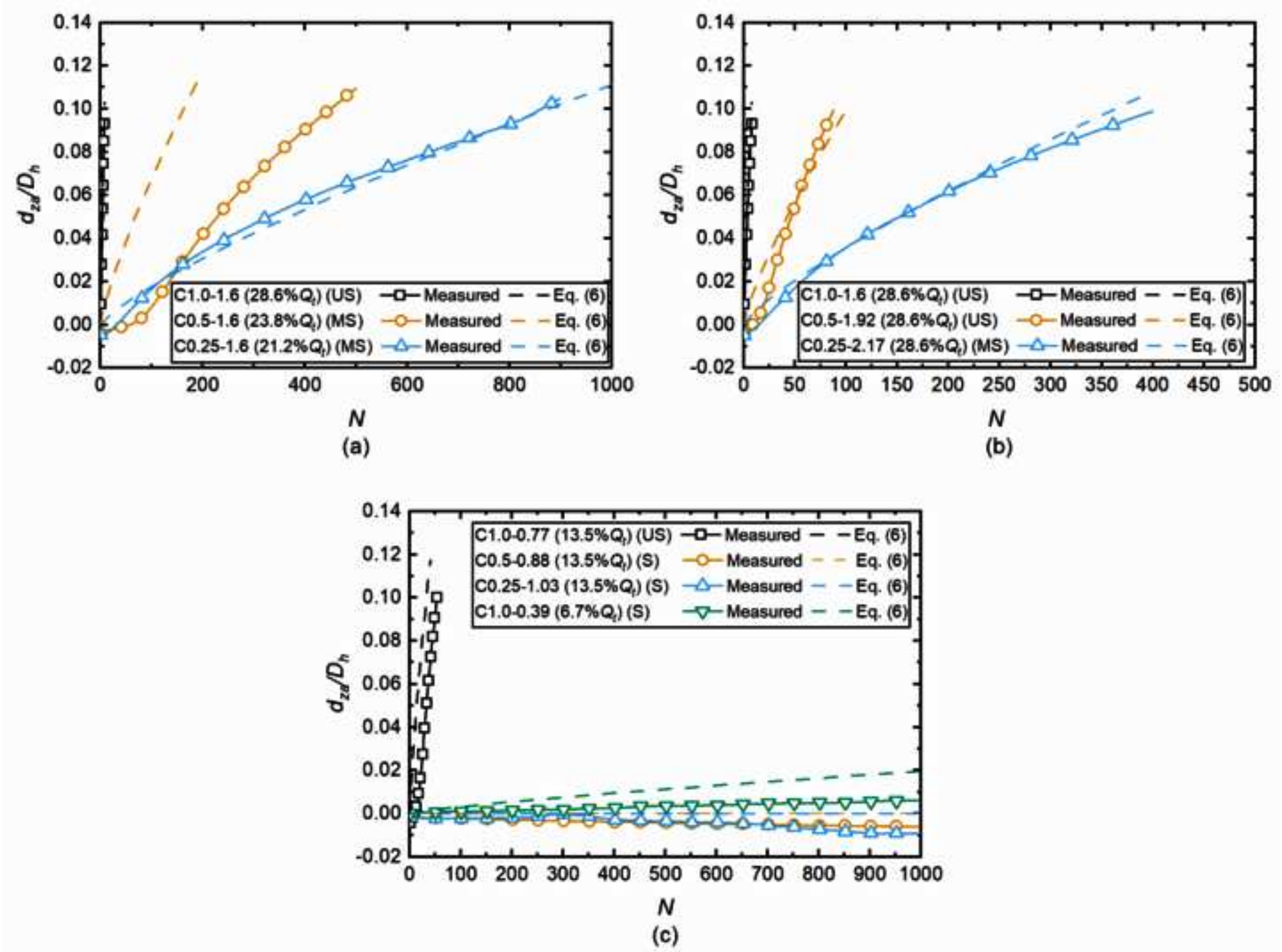

fig 9

Click here to access/download;Figure;fig 9.tif

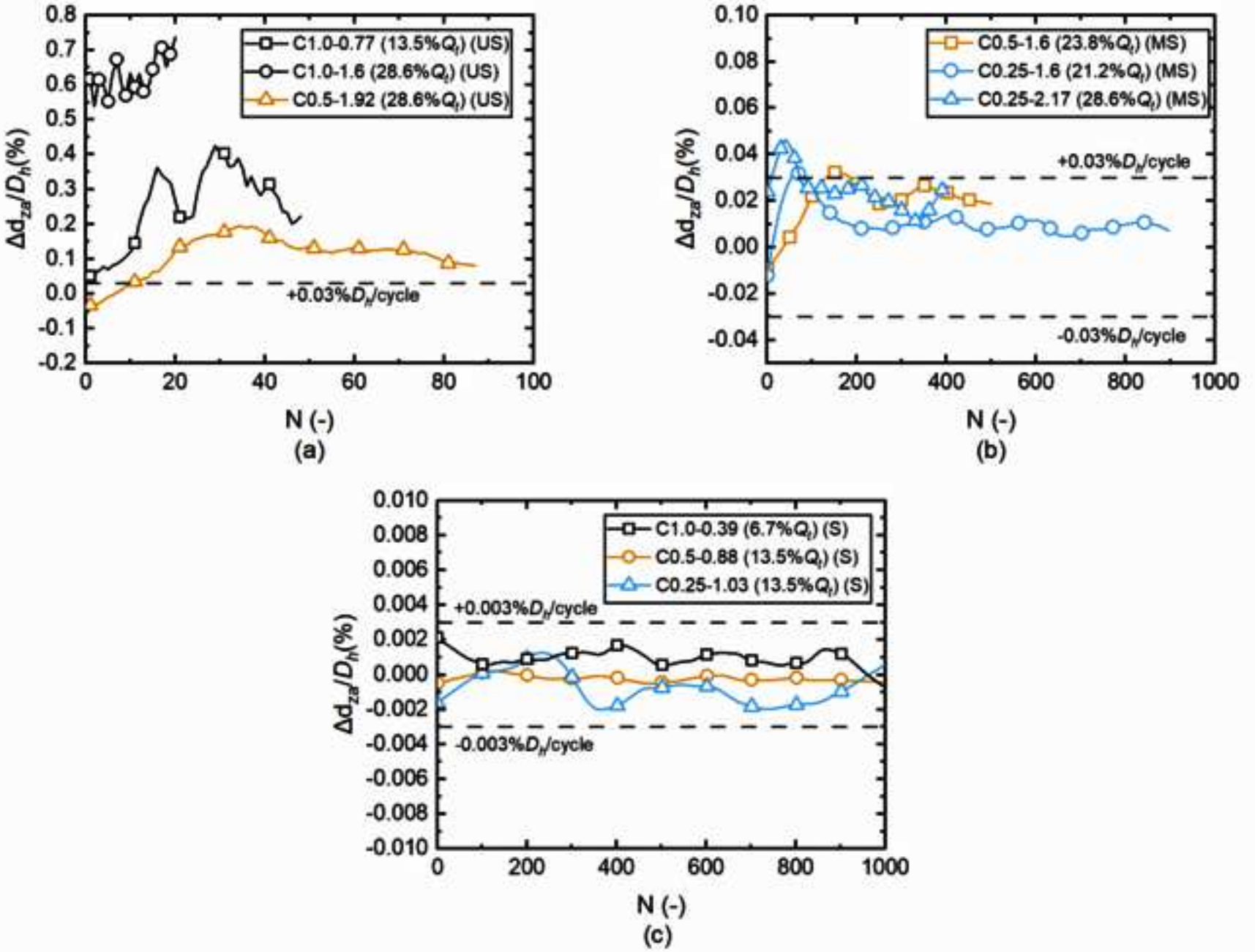

fig 10

Click here to access/download;Figure;Fig 10.tif

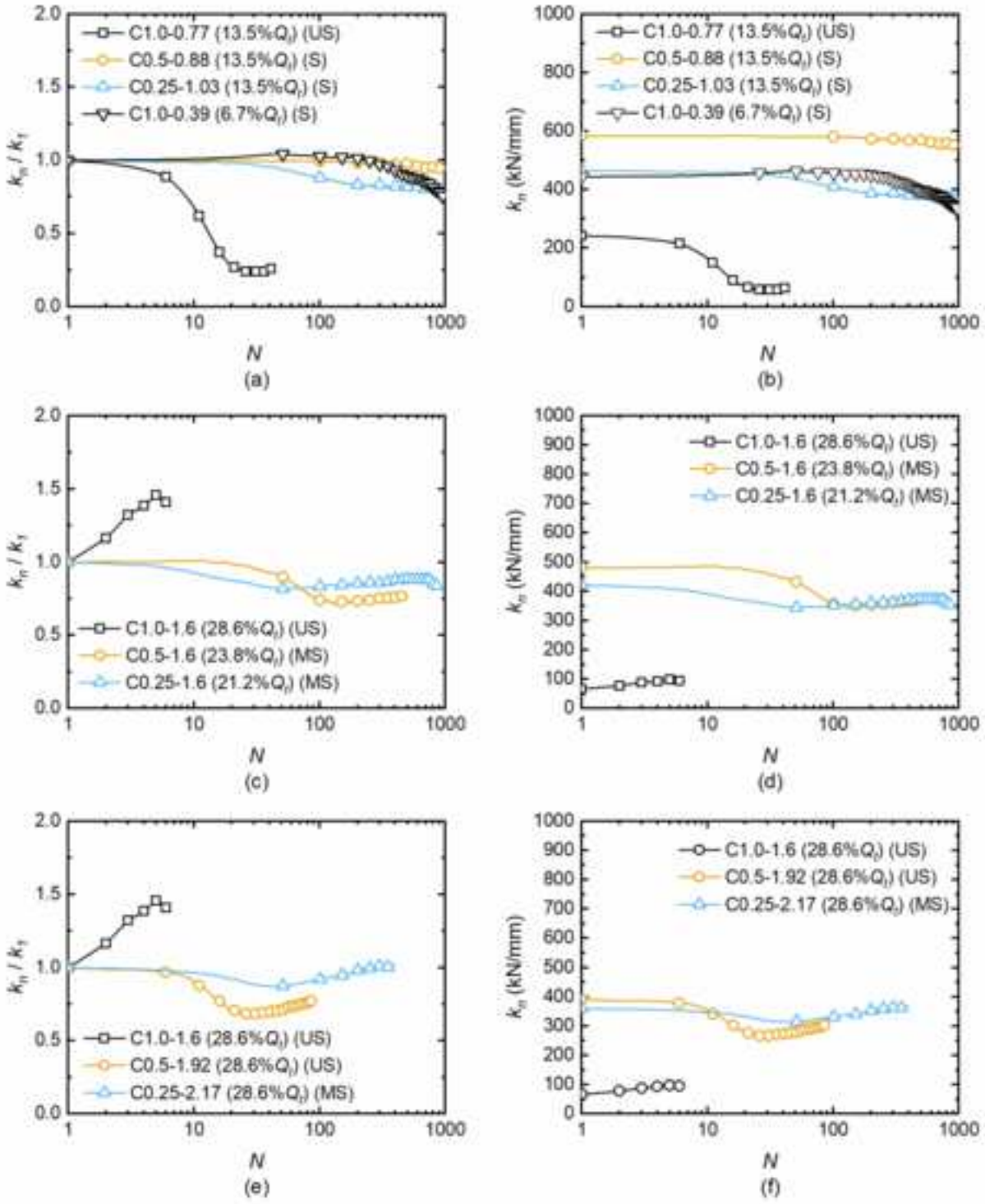

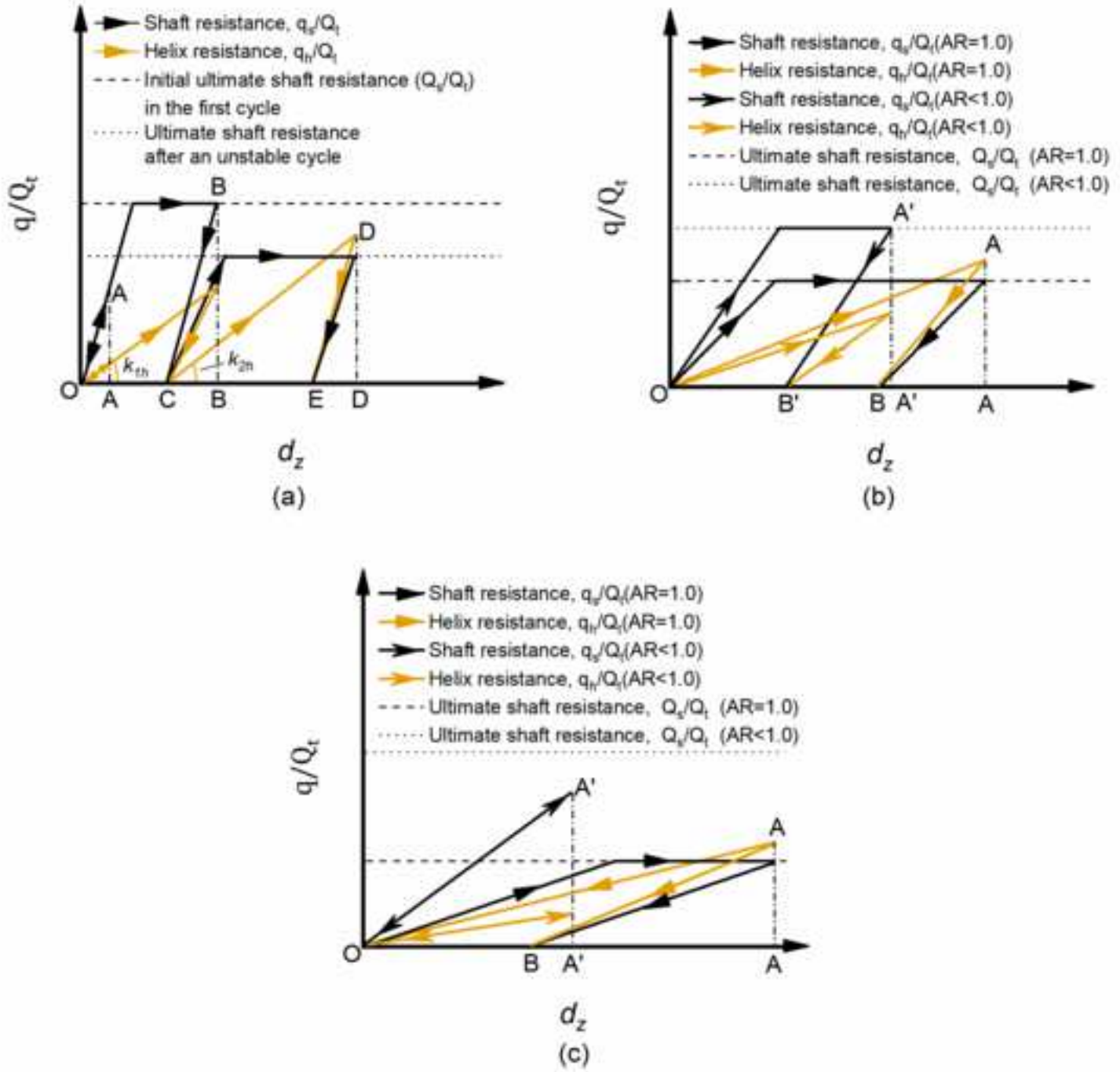

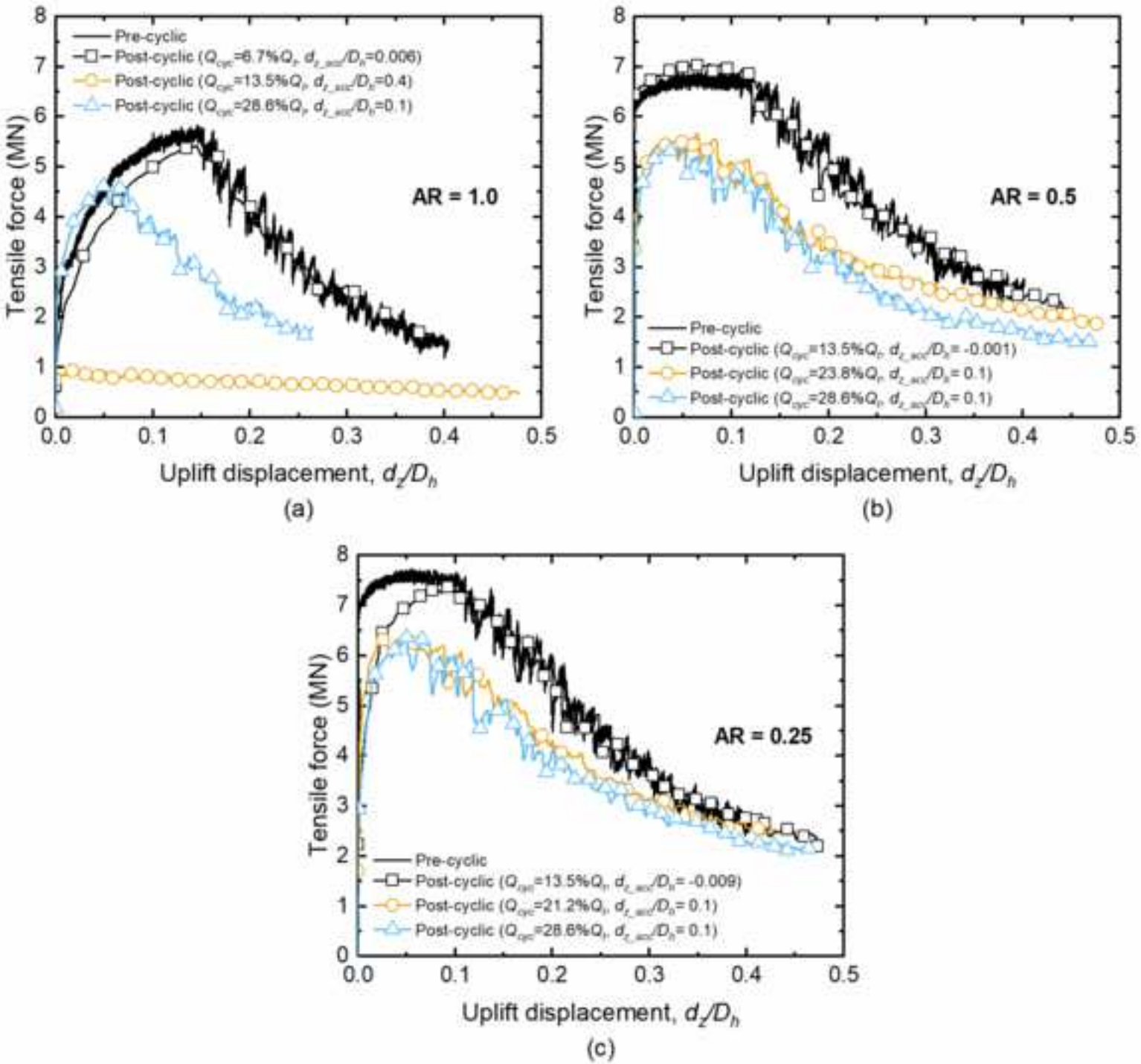

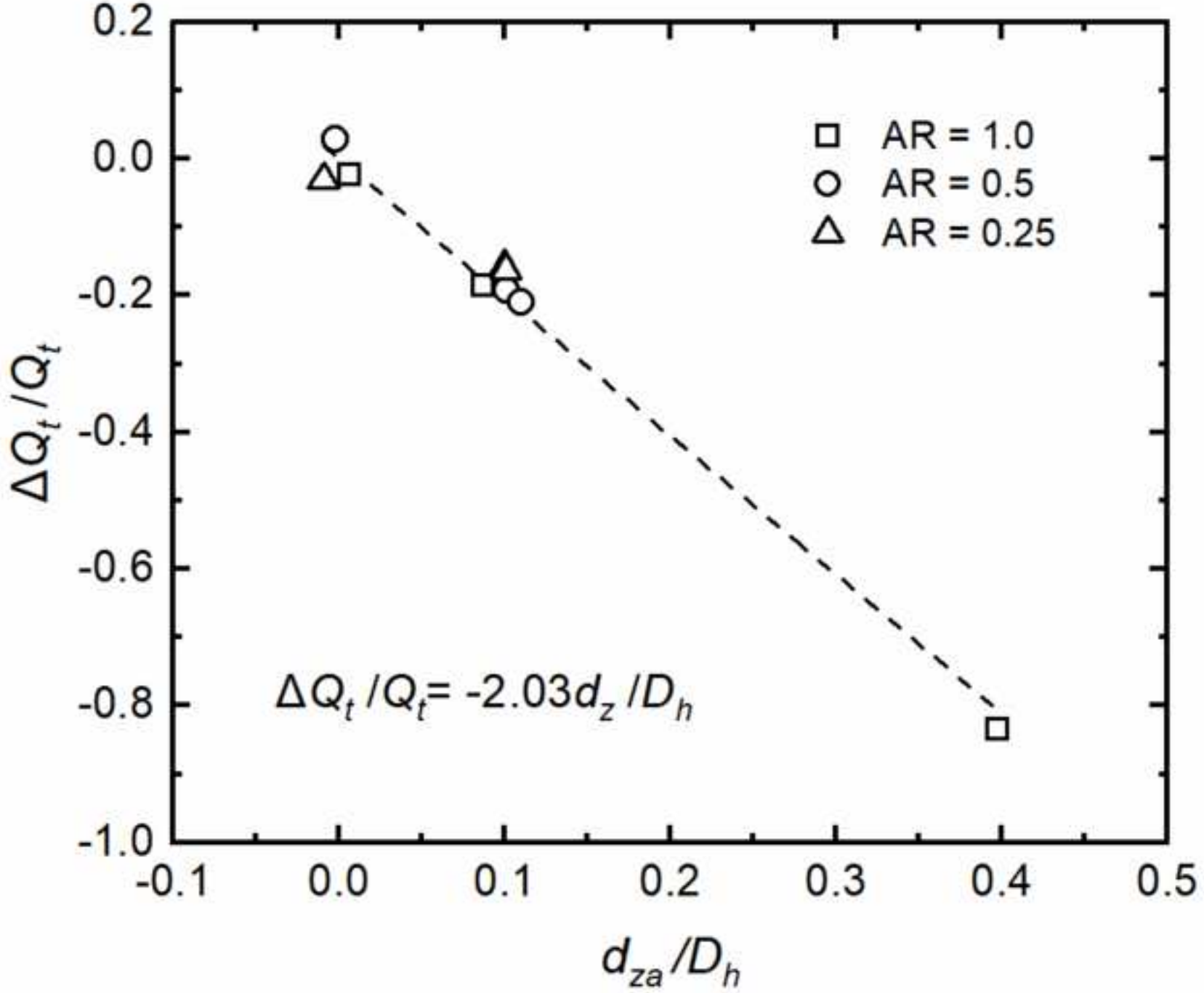

fig 14

Click here to access/download;Figure;Fig 14.tif

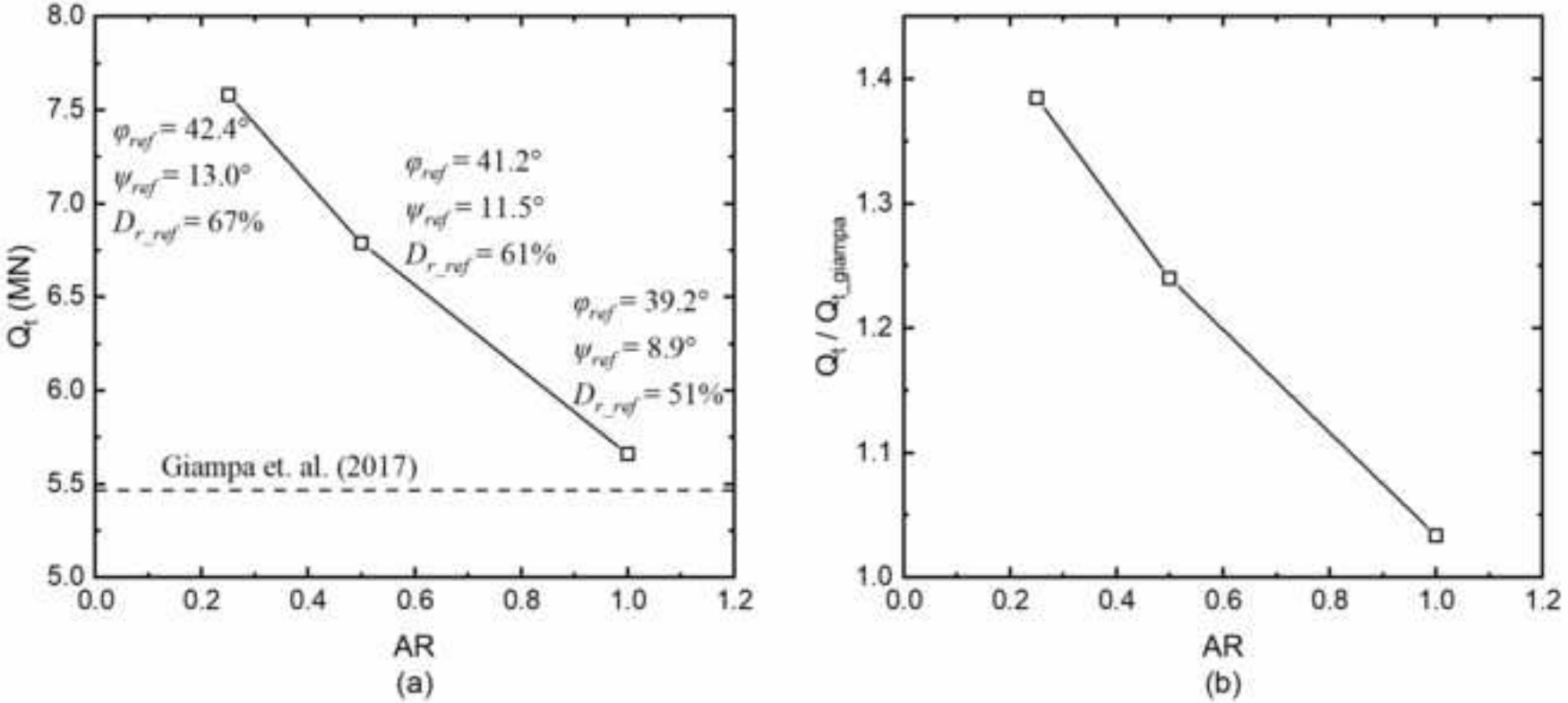

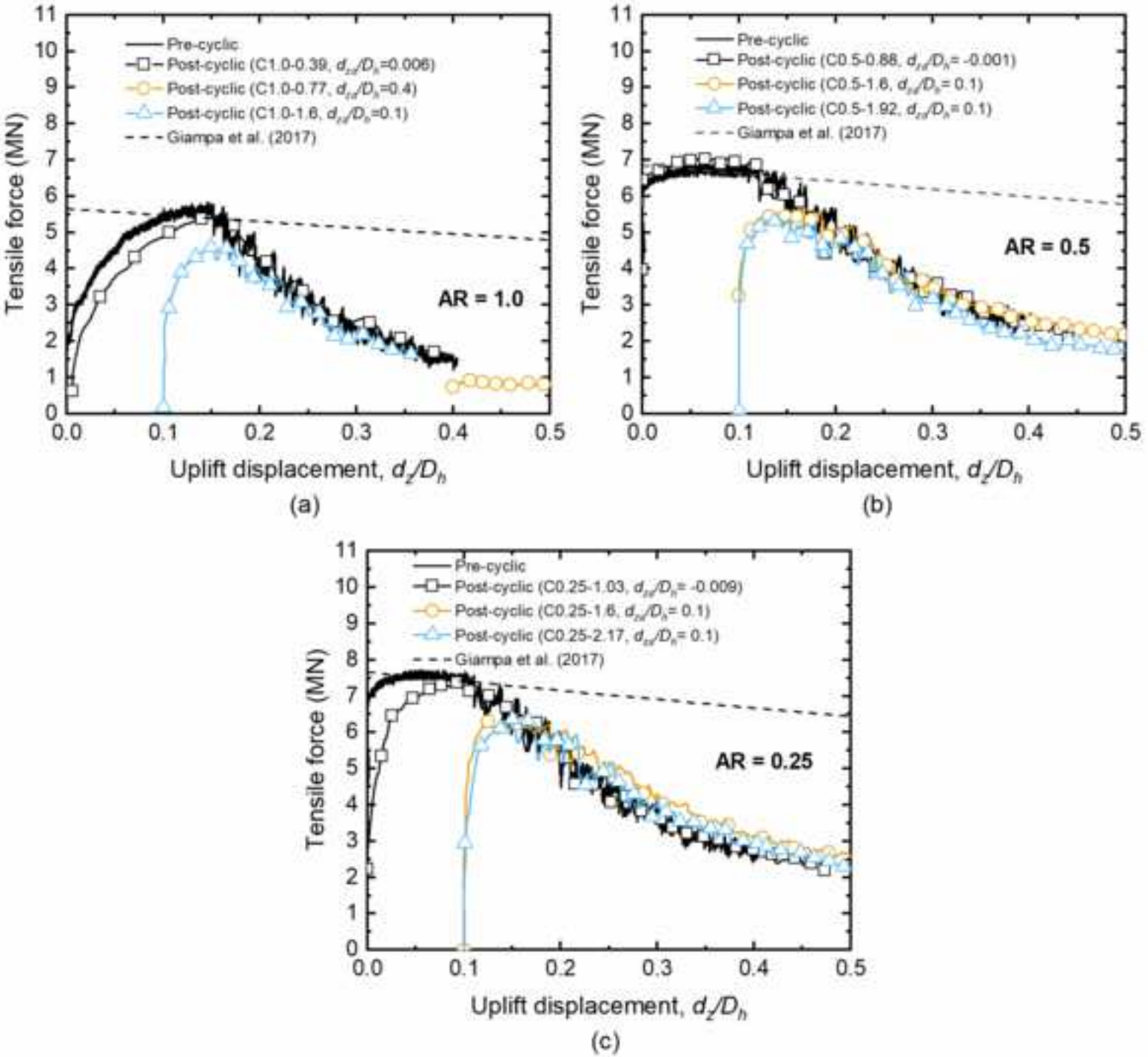

fig 16

Click here to access/download;Figure;Fig 16.tif

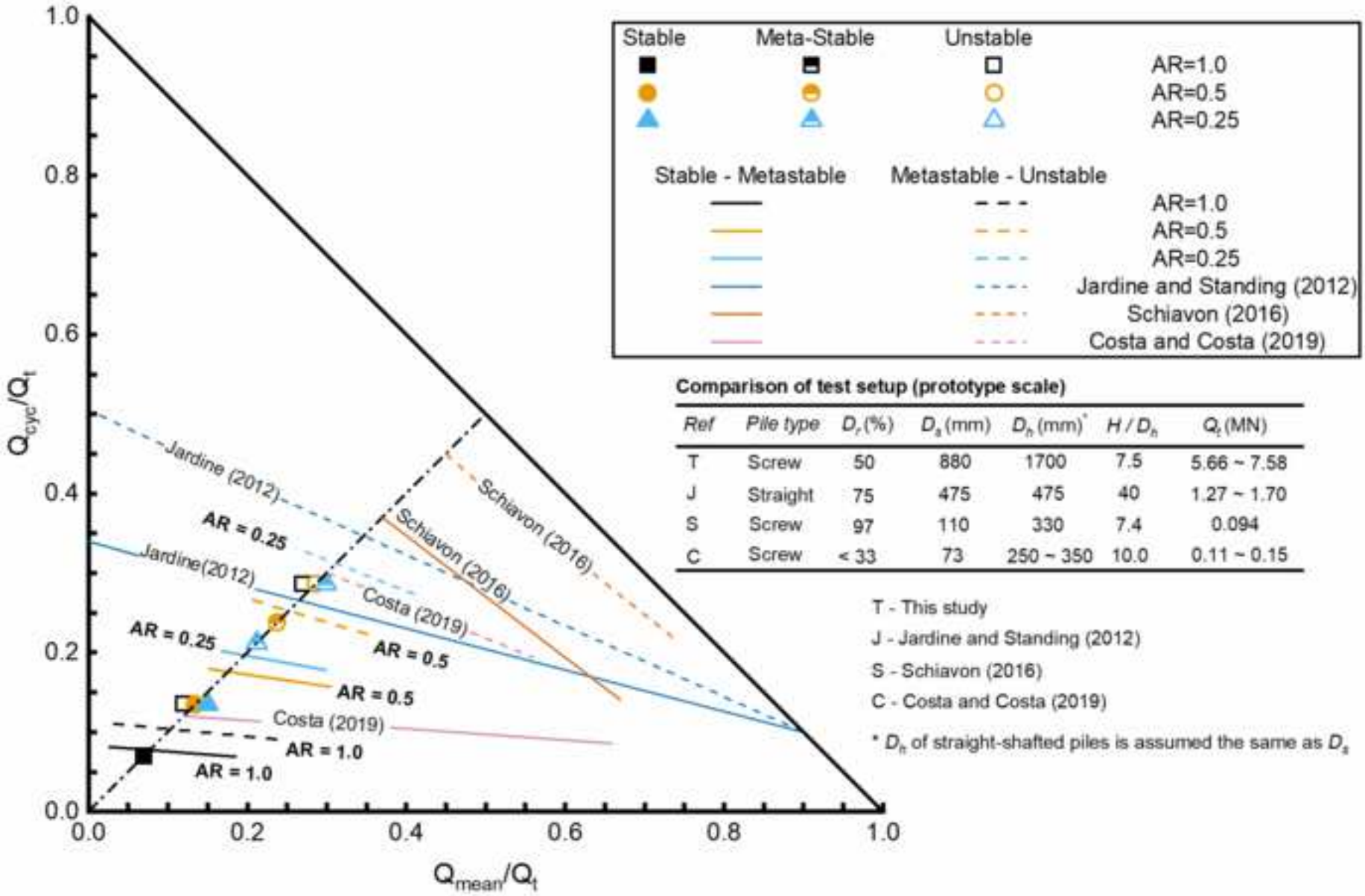

Comparison of test setup (prototype scale)

Ref	*Pile type*	D_r (%)	D_s (mm)	D_h (mm)*	H/D_h	Q_t (MN)
T	Screw	50	880	1700	7.5	5.66 ~ 7.58
J	Straight	75	475	475	40	1.27 ~ 1.70
S	Screw	97	110	330	7.4	0.094
C	Screw	< 33	73	250 ~ 350	10.0	0.11 ~ 0.15

T - This study

J - Jardine and Standing (2012)

S - Schiavon (2016)

C - Costa and Costa (2019)

* D_h of straight-shafted piles is assumed the same as D_s

fig 17

Click here to access/download;Figure;fig17.tif